A PROJECT REPORT ON

SNOW AND GLACIER CHANGES AND THEIR IMPACTS ON MELT RUNOFF IN HIMALAYAN BASINS

(NIH Internal Study)

THE STUDY TEAM

Dr. Vishal Singh, Sc "D"

Dr. Sanjay K. Jain, Sc "G" (Retired)

NATIONAL INSTITUTE OF HYDROLOGY

JAL VIGYAN BHAVAN

ROORKEE - 247 667 (INDIA)

MARCH 2022

TABLE OF CONTENTS

LIST OF FIGURES

(d) regression plots showing comparison between observed snow and modelled snow-covered areas (%) during 2018.

Figure 9: Comparison of SCAs (%) between SPHY and MODIS corresponding to each elevation zone (EZ) during 2010.

Figure 10: Time series and regression plots showing the comparison between simulated streamflow (including snowmelt and glacier melt) against observed streamflow at Sangla gauge during: (a, b) 2003-2010 and (c, d) 2011-2018.

Figure 11: Average annual scenarios of main water balance components such as simulated runoff (Sim Q), Glacier melt runoff (Glacier Q), Snowmelt runoff (Snow Q), rainfall induced runoff (Rain Q) and runoff from the baseflow (Base Q) simulated by SPHY during (a) 2003-2010 and (b) 2011-2018.

Figure 12: Annual variations in Sim Q, Rain Q, Snow Q, Glacier Q and Base Q computed in during 2003-2018

Figure 13: Shows the distribution and amount of runoff components viz. snow Q, glacier Q, rain Q and base Q vary from upstream watersheds to downstream watersheds.

Figure 14: Shows decadal changes in different runoff components at Sangla.

Figure 15: Variations in Sim Q (a), Glacier Q (b), Snow Q (c) and Rain Q (d) computed during two times i.e. 2003-2010 and 2011-2018.

Figure 16: Monthly variations in Sim Q, Snow Q, Glacier Q and Rain Q during the time series sets 2003-2010 (a, c, e, g) and 2011-2018 (b, d, f, h).

Figure 17: Month wise variations and trends in Sim Q, Rain Q, Glacier Q and Snow Q: (a) variations in Sim Q and Rain Q, (b) variations in Glacier Q and Snow Q.

Figure 18: Annual variations and trends in Snow Q and Glacier Q across 17 stations out of 30 stations dominated with snow and glaciers during 2003-2018.

Figure 19: Monthly variations in (a) Glacier Q and (b) Snow Q across 17 stations dominated with snow and glaciers during 2003-2018.

Figure 20: Highlighting changes in glacier maps during (a) 2000, (b) 2006, (c) 2011, (d) 2018 and (e) comparing variations in glacier maps corresponded to elevations.

Figure 21: Glacier area and glacier melt runoff (glacier Q, daily mean in m^3/s) changes as per selected watersheds comprises with large size and small size glaciers in BRB.

Figure 22: Shows the long-term change in snow cover (%) in the Historical time during 1951-2014.

Figure 23: Shows the long-term change in snow cover (%) during 2015-2100 as per (CMIP6 Models) SSP245.

Figure 24: Figure 2: Shows the long-term change in snow cover (%) during 2015-2100 as per (CMIP6 Models) SSP245.

Figure 25: Shows the annual average trends and changes in different runoff components are the Sangla gauge under different CMIP6 scenarios: SSP245 and SSP585.

LIST OF TABLES

ABSTRACT

Monitoring the changes in glaciers and their impact on melt runoff is significant to assess the availability of water resources in the Himalayan basins. In this study, the spatial processes in Hydrology (SPHY) model was incorporated with variable degree-day factors coupled with temperature index model in the Baspa River basin, a major tributary of Satluj River, located in Western Himalaya. The temporal glacier maps derived from the LANDSAT satellite sensors and Moderate Resolution Imaging Spectroradiometer (MODIS) derived snow-covered area (SCA) maps have been used to compute the snow and glacier melt runoff separately. The SCA maps generated through the model were found comparable to the MODIS derived SCA maps for the years 2000 and 2008. Model simulation results showed that SPHY based computed discharge at the outlet i.e. Sangla gauge was found satisfactory when compared to the observed discharge and R^2 computed > 0.7. The contribution from glacier melt runoff has been found to be reduced from 18 to 12% while snowmelt contribution increased from 58 to 64% from 2000 to 2018. On the basis of analysis of the 17 watersheds (i.e. dominated by snow and glaciers) out of 30 watersheds created in the basin, the glacier melt runoff in glacier dominated watersheds is increasing while in other watersheds it is reducing due to reduced glacier cover. On an average, glacier melt runoff has decreased 14% and 44%, snow melt increased 24 and 42% and rainfall runoff 31 and 40% for the year 20011 to 2018 with respect to the year 2003 from these 17 watersheds. As per SPHY, corresponding to glacier map of the year 2000, the glacier ice volume has been computed around 13.41 km^3, while for the glacier map of 2018, it has been reduced around 10.99 km^3.

Considering the climate change impacts through CMIP6 model scenarios, the comparative assessment of snow cover and runoff components under historical, SSP245 (i.e. moderate emission scenario) and SSP585 (i.e. high emission scenario) scenarios reveals noteworthy changes. The historical time period (1951-2014) shows relatively stable snow cover and runoff

patterns, with snowmelt being the dominant source of water. Although, projections under SSP245 and SSP585 indicate profound shifts in snow and glacier induced changes in terms of snow cover and runoff. Under SSP245, moderate emissions lead to a gradual decline in snow cover and snowmelt runoff, with increases in rainfall and glacial melt contributing more significantly to total runoff. Snowmelt decreases by 14.75% and 44.45% in the near and far future, respectively, while glacial melt and rainfall increase substantially. The scenario reflects a slow but steady transition from snow-driven to rain and glacier-driven runoff, particularly after 2050. In contrast, SSP585, with higher emissions, shows much more drastic changes. Snow cover and snowmelt decline sharply, with a 53.77% reduction in snowmelt runoff by 2090. Rainfall and glacial melt increase significantly, especially after mid-century, resulting in more extreme total runoff fluctuations.

CHAPTER 1

INTRODUCTION

Cryosphere is a significant component of Earth's systems. The glacier-related feedback mechanisms govern atmospheric, hydrospheric and lithospheric response (Bush, 2000; Shroder and Bishop, 2000; Meier and Wahr, 2002). The earth's surface has been influenced repeatedly over the past three million years by long periods of glaciations, separated by short warm interglacial periods. Approximately 47 million sq. km area of the earth was covered by glaciers during peak glaciations, which is estimated to be three times more than the present ice cover over the earth (Price, 1973). On planet Earth, there is about 26 million km^3 of ice at present, contributing almost 10% to the world's land area1 coverage. In the Himalaya, approximately 33,000 km^2 area is covered by the glaciers (Dyurgerov and Meier, 1997) with a total number of 9,600 glaciers in the Indian Himalaya (Raina and Srivastava, 2008) which is one of the largest concentrations of glacier-stored water after the Polar Regions (Kulkarni and Buch, 1991). Himalayan glaciers are an important source of water of the North Indian Rivers during critical summer months. Water discharge from Himalayan glaciers contributes to the overall river runoff (Immerzeel et al., 2010) and water discharge from Himalayan glaciers is important for irrigation and hydropower generation (Singh et al., 2009).

Glaciers are considered a key indicator of climate as they often react sensitively to climate change (Oerlemans, 1994). Widespread glacier retreat in many parts of the world supports this (Bolch et al., 2007; Schneider et al., 2007; Pan et al., 2011). Alpine glaciers are also thought to be very sensitive to climate change within the Himalaya, due to the altitude range and the variability in debris cover (Nakawo et al., 1997). It is therefore, necessary to map and monitor alpine glacial fluctuations from the perception of climate-change (Bishop et al., 2004).

Like in many other parts of the world, most of the Himalayan glaciers are shrinking (Kadota et al., 2000; Ren et al., 2006; WWF, 2005). Since 1850s, the Himalayan glaciers are in a general state of recession (Mayewski and Jeschke, 1979; Bhambri and Bolch, 2009). Over the past few decades, an increased receding trend has been exhibited by Himalayan glaciers as depicted by several past studies (Kukarni et al., 2005 and 2007; Bolch et al., 2008; Chaujar, 2009, Mehta et al., 2011). Approximately, retreat of a kilometre has been shown by the Himalayan glaciers since the Little Ice Age (Mool et al., 2001). Simultaneously, since the late 20th century, the Earth's surface temperature has risen dramatically (Solomon et al., 2007). From the north-western Himalayan region, the weather data records have depicted an increase of about 1.7 ºC in temperature over the past century and a decreasing trend in monsoon precipitation (Bhutiyani et al., 2007 and 2009). These changes are documented by periodic inventories of the glaciers. Now, remote-sensing techniques using satellite data are also used for monitoring glacier extent and changes (Bishop et al., 1998; Silverio and Jaquet, 2005; Strozzi et al., 2008; Bhambri et al., 2011), and for establishing databases to assess these changes at regional and global scale (Kollmeyer, 1980; Bishop and Shroder, 2004; Raup et al., 2007, Bolch et al., 2010). In addition, for improving our knowledge of glacier response to climate change, regular monitoring of a large number of glaciers is important globally including the Himalayas. However, due to the rugged and inaccessible terrain and also larger number of glaciers, the use of conventional methods for monitoring of Himalayan glaciers is normally difficult. Some field-based records have been made at selected Himalayan glaciers. This may not provide a complete and representative scenario of glacial retreat. Multitemporal and multispectral satellite data provide abundant potential for mapping and monitoring the large spatial coverage of glaciers at regular temporal intervals, as they allow semi-automated glacier mapping (Paul et al., 2009; Racoviteanu et al., 2009; Bolch et al., 2010).

As mentioned, several mapping and monitoring studies exist for the Himalayan glaciers and a few studies have also been published on the mapping and variability of the Baspa basin glaciers (e,g, Kulkarni et al., 2002 and 2003; Raina and Srivastava, 2008). The present study examines mountain glacier changes in Baspa River basin over the past 40 years and comparatively evaluates air temperature, snow water equivalent and precipitation trends. Changes in areal extent and volumes are used as indices to measure glacier changes. Survey of India (SOI) topographical maps and Landsat Enhanced Thematic Mapper Plus (ETM+) datasets have been used to map these changes.

1.1 Characteristics of glacier and climate change

During recent decades, the climate change impact studies associated with global warming has been given ample attention worldwide. As per the IPCC, (2007), by the end of this century, the temperatures are mostly likely expected to increase by 1.8-4°C (3.2-7.2°F). After the industrial revolution of the developed world, the continuous increase in Global temperatures since 1750s, has fuelled the notion that the Earth's warming is most likely due to the anthropogenic activities. In India, Gangwar, (2006), has reported that the trend of climate change has shown a sudden acceleration in pace after 1971. Eleven of the warmest years were recorded since 1990, with 2005 as the warmest on record (ICIMOD, 2007). Like other regions, the most obvious and clear impact of climate change, is certainly the widespread melting and retreat of Himalayan glaciers (Scherler et al., 2011). The glaciers respond more sensitively to climatic variations than most other ice bodies on surface of the Earth (Kääb et al., 2007). Therefore, the glaciers especially mountain glaciers are considered the key indicators of climate change particularly in remote areas (IPCC, 2007). However, the wide spread debris-covered Himalayan glaciers exhibit different patterns of dynamics (Scherler et al., 2011).

The retreat may be identified through the observation and demarcation of lateral and terminal moraines which generally indicate the wide spread historical extents of glaciers. In

addition, the recent glacier fluctuations are easily observed through the changes in surface area/length and variable positions of the snout of the glaciers. However, the area/length changes give a filtered signal of the climate change as the glacier requires adjusting to the changing situation generally called as response time. The response time varies for each glacier and depends mainly on its thickness and the overall climatic conditions. For example, the dynamic response time for glaciers in a temperate climate having a thickness of 150-300 m is 15-60 years (Bahr et al., 1998). Normally, the response of glaciers to climatic fluctuations is a complex phenomenon. The response of glaciers also depends on the non-climatic factors such as the ice dynamics, glacier hypsometry and topographic parameters.

Basically, the mass balance is the key and important parameter to observe about the health of the glaciers as it is the direct and sensitive signal of climatic fluctuations. The mass balance studies deal with the mass of a glacier and the distribution of its changes in space and time (Paterson, 1994). Under warming conditions, the positive mass balance of glaciers may result in glacier advance, if the warming occurs mainly in the winter months due to the occurrence of more solid precipitation. Over a one hydrological year, the altitude where; accumulation balances ablation is known as the equilibrium line altitude (ELA). The ELA is an important characteristic feature of a glacier and on an annual basis; the ELA reacts to a combination of climate variables, particularly air temperature and precipitation. Hence, a glacier may advance or retreat even if the net mass balance is zero. If the net balance equals zero over many years the glacier is determined to be in a steady state. Another typical characteristic of the glacier is its motion which can be distinguished as glacier flow and basal motion. Overall, the motion depends on the topographic conditions, mass gain and the climate. However, it is interesting to note that some glaciers, advance suddenly with much higher velocities leading to a phenomenon, called as glacier surge.

1.2 Impacts of climate change

In the high mountain areas of the world, the role of snow and ice as an important source of freshwater has been highlighted by several ealier studies (e.g., Kaser et al., 2010; Immerzeel et al., 2010). The glaciers are the most sensitive records of climate changes and active geomorphic agents in shaping the landforms of glaciated regions. The glacial landforms are the direct imprints of past glaciations, providing reliable proof of the evolution of the past cryosphere and contain important information on climate variables as well. There are serious concerns about the potential impacts of re**d**uction of snow and glacier under warming climate on the social and economic development (Barry, 2006; Adeloye and Ojha, 2010) with its hydro-ecological consequences to surrounding communities (Kehrwald et al., 2008; Milner et al., 2009) and wide implications for decision makers (Adeloye, 2013). The climate change has also its influence on the functionality of dams and reservoir characteristics (Soundharajan et al., 2013). Importantly, the loss in Alpine glaciers may have a severe impact on the regional water supplies (Kaser et al., 2010), contribution to sea level rise (Kaser et al., 2006), and increased related hazards such as outburst floods from moraine-dammed lakes (Du et al., 2012). These abrupt-onset floods symbolize high-magnitude, low-frequency catastrophic phenomena and have massive potential for geomorphological reworking along the channels and floodplain environments (Worni et al., 2012; Westoby et al., 2014).

1.3 Scope of the study

Snow and glaciers in the Himalaya and Trans- Himalayan Mountain belt are nearest to Tropic of Cancer and hence, heat up more than the Arctic and Antarctic ice sheets or other temperate glaciers. Thus, these glaciers provide a distinctive opportunity to understand the changes in area, thickness, mass balance, their consequences on water resources and related hazards, changes in length and snout fluctuations that can be modeled for different types of climatic regimes. However, due to the lack of comprehensive ground-based observations

(Winiger et al., 2005); detailed knowledge on snow and glaciers behavior under different climatic patterns is limited (Wagnon et al., 2007). Similarly, the quantitative assessments of the different hydrologic components and their relative contribution to overall river discharge are rare and include large uncertainties (Singh and Jain, 2003; Kumar et al., 2007b). However, recent advances in glaciological and hydrological research that are based on time series of high-resolution remote sensing data that account for the high spatial heterogeneity of climate and surface processes in alpine terrain has made it possible to get a brief comprehension (Molotch and Norte, 2009; Bookhagen and Burbank, 2010). Accurate assessments of major glaciological and hydrological components are vitally important, because they define the boundary conditions and thus result in an outcome of any modeling study addressing climate change impacts in the Himalaya (Akhtar et al., 2008; Immerzeel et al., 2010).

To understand and predict the response of glaciers to climate change with its impacts on sea level change, watershed hydrology and glacier-related hazards, continuous monitoring of glacier changes is an important aspect. Furthermore, the climatic stations in the altitude of glaciers are rare and the climate-glacier relation needs to be better investigated in order to fully understand the glaciers feedback. Similarly, to predict and mitigate the socio-economic impacts of climate change, rigorous assessment and quantification of links existing between the glacier, snow cover, climate and hydrology is very imperative. In addition, this has necessitated the assessment and monitoring of potentially hazardous glacial lakes through the use of remote sensing, especially in high mountainous areas due to inaccessibility and lack of field surveys (Quincey et al., 2005). The Geoinformatics provides the pragmatic approaches to carry out the all kinds of geoenvironmental studies (Pirasteh et al., 2011, Yusof et al., 2011**)** and offer great opportunities in the Himalaya and in areas lacking traditional field-based glaciological methods. Although, in the Indian Himalaya, the number of glacial lakes present, are not as well-known currently. But the glacial lakes are developing at an increasing and threatening rate

in response to continuous glacier recession and hence, can be disastrous in near future (Benn et al., 2001). Thus, in the Indian part of Himalaya, a large research gap exists in modeling potential hazards related to existing and future glacial lakes.

CHAPTER 2

THE STUDY AREA AND DATA SOURCES

2.1. Baspa Basin

Baspa River is a major tributary of the great river Satluj which originates from Tibet in Great Himalayan Mountain Range at an elevation of more than 5141 meters above mean sea level. A few km downstream of the Indo-China border Satluj river meets its biggest tributary, the Spiti River, joining Satluj from a north-westerly direction and having its source close to Kunjamla. After the confluence with Spiti river, Satluj river takes a some 70 km run through Kinnar in a South-Westerly direction until its confluence with its second major tributary, Baspa river, which joins it from South-Eastern direction.

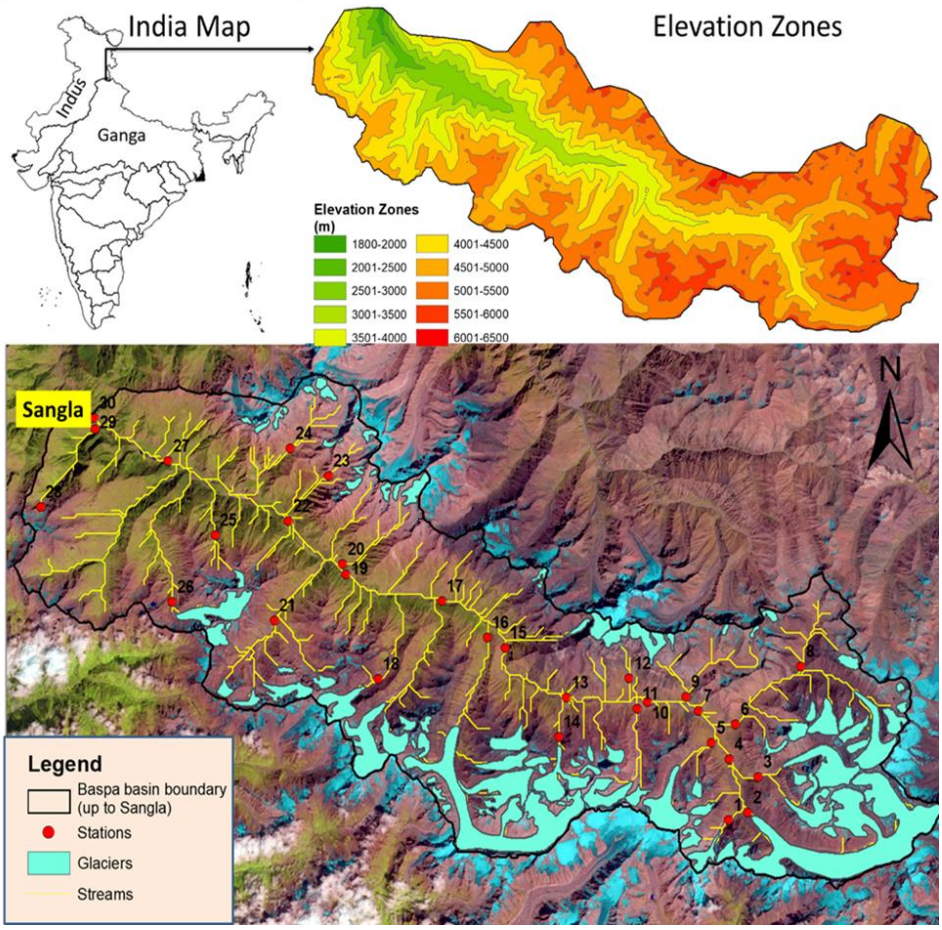

Figure 1: Showing location, study area, glaciers, elevations and other features of the Himalayan Baspa River basin (up to Sangla gauge).

Several nallas and khuds contribute to its flows. Prominent among these are Arssomang, Maosu, Janapa, Rimdarang, Shusang, Sigan, hurba and Hania. Numerous glaciers also drain into it, most important being Saroo glacier on the right bank, and Hania and Billare glaciers on the left bank. After flowing for a length of 66 km, the Baspa ultimately joins the Satluj. Gross elevation difference from the origin of the river up to its confluence with the Satluj is 2825 m. Such a considerable drop within a short distance offers very favourable condition for hydropower development. Catchment area of the river Baspa at the proposed barrage site at Sangla is ~1100 sq km. The catchment is elongated and leaf shaped.

The Baspa River basin is located in Kinnaur District, Himachal Pradesh, India and stretches between 31º 05' to 31º 30' N latitude and 78º 00' to 78º 50' E longitude. The Baspa River is a major tributary of the Satluj River, which drains eastern part of the Himachal Pradesh. The river originates at Arsomang and Baspa Bamak glaciers and travels 72 km through the valley before joining the Satluj River at Karcham. The location map of the Baspa basin is shown in Figure 1. The basin is comprised of valley glaciers that vary in form from simple to compound glaciers of varying sizes. The basin is highly glacierized and located in the higher-altitude range, and is west flowing with most of the glaciers located in the northern slope of the Pir Panjal Mountain range. The main glaciers of the Baspa valley are Baspa Bamak, and Shaune Garang, Joya Garang and Karu. Due to high altitude, the stream flow is mostly generated from snow and glaciers melt runoff. In socio-economic terms, the Baspa Basin is important as many mini and micro-hydropower stations are being planned in this basin. Therefore, it is important to monitor the variations in glaciers for the Baspa Basin.

Table 1: Characteristics of the Himalayan Baspa River Basin.

SI. No.	**Characteristics**	**Baspa Basin**
1	Selected Study Area (Km^2)	1100
2	Mean Elevation (m)	4092
3	Maximum Elevation (m)	6442

4	Minimum Elevation (m)	1742
5	Number of Glaciers	109
6	Glacier Area (RG6.0)	230.74
7	Glacier Area Delineated in Different Years	221.17(2000), 176.96(2018)
8	Glacier Area (%) covered with Clean Ice	75-78
9	Glacier Area (%) covered with Debris	22-25
10	Average Snow Cover Area Max/Min (%) - MODIS	95.12 (Jan)/36.81 (Jul)
11	Average Snow Cover Area Max/Min (%) - SPHY	98.71 (Jan)/46.47 (Jul)
12	Annual Precipitation (mm)	800mm - 1400mm
13	Average Annual Min/Max Temperature (°C)	(-11°C /28°C)
14	Annual Average Glacier Melt Flow at Outlet (m3/s)	4.34
15	Annual Average Snowmelt Flow at Outlet (m3/s)	25.31
16	Annual Average Rainfall Flow at Outlet (m3/s)	10.03
17	Annual Average Base Flow at Outlet (m3/s)	5.26
18	Annual Average Total Flow at Outlet (m3/s)	45

2.2 Data Used in the Study

In this study, to setup the SPHY model various thematic data layers such as landuse/landcover (LULC) map, soil map, digital elevation model (DEM), real time snow covers, glacier maps and meteorological parameters such as daily precipitation, daily minimum and maximum temperature, daily average temperature have been used. The GlobCover moderate resolution LULC map (prepared in 2009) has been utilized. The Globcover dataset is available freely and can be obtained from ESA website in GeoTIFF Format in the World Geodetic System 1984 (WGS 84) coordinate system at 10 arc-seconds (~300 m) spatial resolution (http://due.esrin.esa.int/page_globcover.php). In this study, a high-resolution soil map of hydraulic properties (HiHydroSoil version 1.2, 2016) based soil map has been utilized (http://soilgrids1km.isric.org/). The details about the soil map and their parameters are given by de Boer (2016). For DEM, Shuttle Radar Topographic Mission (SRTM) based DEM with 30 m spatial resolution has been utilized for the extraction of topographic parameters (https://earthexplorer.usgs.gov/).

For the meteorological datasets, Indian Meteorological Department (IMD) gridded datasets ($0.25^{O}\times0.25^{O}$) and Climate Hazards Group InfraRed Precipitation with Site data (CHIRPS) available at 0.05^{O} resolution scale have been utilized (Gupta et al., 2019; Prakash, 2019). Both the datasets have been interpolated at the same scale ($0.05^{O}\times0.05^{O}$) and then the quantile regression based on cumulative density function (CDF), a bias correction method, has been applied to correct the CHIRP precipitation with reference to IMD precipitation datasets. As per previous studies, the quantile mapping method has been found the best method for the bias correction of the precipitation datasets (Singh and Xiaosheng, 2019; Cannon et al., 2015). The reliability of CHIPS precipitation data has already been evaluated by few researchers across India and they resulted that CHIRPS performed superior among other global precipitation datasets, especially in capturing precipitation extremes (Gupta et al., 2019; Prakash, 2019). Total 15 precipitation grids have been found closer to the study area and hence utilized. For re-gridding and bias correction, python programming based Xarray and NumPy modules have been utilized (Byers et al., 2018). Daily minimum, maximum and average temperature data was obtained from IMD has been utilized for the analysis. For model calibration, the observed discharge (2003-2018) available at Sangla gauge has been utilized.

For the preparation of glacier maps, Landsat MSS TM, ETM+, TM and Landsat 8 satellite sensors-based dataset have been utilized. Fortunately, for the year 2006, the selected study area was in the center of ETM+ scene, almost not affected by scan line errors (SLE) (Mir et al., 2017). For snow covers extraction, MODIS (MOD10A2) having 500 m spatial resolution datasets from 2003 to 2018 were downloaded (https://nsidc.org/data/MOD10A2) and processed to extract snow covered area by adopting the methodology as previously used by Shukla et al. (2017). The snow-covered area (SCA) evaluation has been done on the monthly scale and therefore MODIS 8-daily scenes were processed and then aggregated at the monthly scale (Hall and Riggs, 2016).

Table 2: Data available at NASA's GLCF for the study area.

Sensor type	**Resolution**	**Path- Row**	**Acquisition Date**	**Availability**
MSS	79m	157-038	01.12.1979	Snow covered
TM	30m	146-038	10.21.1990	Snow covered
ETM^{+}	30m	146-038	22.10.1999	Available
		146-038	08.10.2000	Available
		146-038	23.09.2006	Available

CHAPTER 3

LITERATURE REVIEW

The Himalaya is unique and highest mountain chain of the world. It is often referred to as the "third pole" (Schild, 2008) and the "water tower of Asia" (Xu et al., 2009). The Himalayan region affects, directly or indirectly, the living of over 300 million people of the Indian subcontinent (Schild, 2008). The region controls flow to the three major river systems; the Ganges, the Brahmaputra, and the Indus. These river systems play an essential role in the economy of many countries including India which depends greatly on it for hydropower, water supply, agriculture, and tourism. However, these delicate Himalayan resources are highly prone to natural hazards, leading to serious concerns especially about current and future climate change impacts on the water stored in snow and glaciers (Cruz et al., 2007). In the region, the climate change concerns are multifaceted encompassing, snow cover changes, glacier retreat, expansion of glacier lakes and glacier lake outburst floods, droughts, landslides, flash floods, (Barnett et al., 2005), agriculture livelihood, human health, biodiversity, and food security (Xu et al., 2009**;** Pirasteh et al., 2010**;** Nakhapakorn and Tripathi, 2005). Thus, regular monitoring of Himalayan cryosphere (snow/glaciers) is important for improving our knowledge of its response to climate change. For this purpose, field investigations are highly suggested. However, keeping in view the time and logistical constraints in such a remote and rugged Himalayan region, only a limited number of glaciers can be monitored. Therefore, techniques of Geoinformatics along with limited field checks appear to be the only means of mapping and monitoring cryospheric fluctuations in this region (Pankaj et al., 2012).

Snow and glaciers covered area and runoff generated due to melt is having an important role in the hydrology of glaciated basin. The Himalaya plays a prominent role in the precipitation and spatial/temporal distribution of runoff through their orographic effect and

water storage in the form of seasonal snow and glacier systems as well as ground water systems (Imeerzeel et al., 2009). Contrary to glaciers, seasonal snow accumulates and discharges water mainly within one annual cycle. The Himalaya has vast resources of snow and glaciers and provides water to the population living in the Indus, Ganges and Brahmaputra basins (Kumar et al., 2018; Kulakrni, 2012; Xu et al., 2009; Singh and Jain, 2002). In comparison to the Ganga and the Brahmaputra, the Indus basin is more dependent on upstream water resources, because of its very arid downstream climate, westerly influenced precipitation regimes and large glacier systems (Lutz et al., 2014; Immerzeel and Bierkens, 2012; Schaner et al., 2012).

As reported, the glacier and snow changes are taking place mainly in response to climatic change. Therefore, in the present research, the trend analysis of various climatic variables was carried out. The study also involves the glacier mapping and change detection studies using geo-spatial techniques. However, the uneven changes in glaciers are attributed to the local topographic and morphometric factors of the glaciers. Thus, keeping these facts in perspective, the present chapter gives a review of the previous studies carried out within the Himalayan region pertaining to climate change which includes glacier and snow changes, changes in climatic variables vis a vis changes in stream flow and glacier lake expansion associated with outburst floods (GLOF). Before this, a brief description of use of Geoinformatics for cryospheric studies is also presented.

3.1 Glacier and snow changes

In the Himalayan region, it is reported that the glacier retreat begun with more gradual climate warming since the Little Ice Age (LIA), which occurred approximately from 1650 to 1850 (Oerlemans, 2005). But, during recent decades, the new and obvious evidence has accelerated the rate of that change (Zemp et al., 2008) and most of the glaciers are dying out to melt in the next 40 years (Chamling, 2005). Majority of the earlier studies showed that the Himalayan glaciers are diminishing and have been in the state of recession since 1850s (Mayewski and

Jeschke, 1979; Bahuguna et al., 2013); with the noticeable exception of the Karakorum region where some glaciers are advancing and is known as Karakorum anomaly (Hewitt, 2005). Recently, Pandey et al., (2011) has reported a retreating trend of 26 glaciers in the western Indian Himalaya from 1975-2007 based on satellite data analysis. Similarly, Scherler et al., (2011) carried out an analysis of satellite data for the monitoring of 286 mountain glaciers from the Hindu Kush, Karakorum, western Indian Himalaya, Tibetan Plateau, West Kunlun Shan, and southern central Himalaya (Nepal, Bhutan, Sikkim, Uttarakhand, and Himachal) during the period between 2000-2008. After analysis, they observed that 58% of studied glaciers under the westerlies-influenced Karakorum region are stable and slowly advancing; while more than 65% of glaciers under the monsoon-influenced regions are receding along with several heavily debris-covered with gentle terminus slope glaciers being stable. Interestingly, they recognized a higher concentration of receding glaciers (79%) in the western Indian Himalayan region and in the northern central Himalaya and West Kunlun Shan (86%) where dominantly debris-free glaciers are present. The rates of retreat are varying between -9.10±5.87 and -14.64±5.87 ma^{-1} and most retreating glaciers are located at elevations of 4700-6400 m amsl (Nie et al., 2010). The glacier changes studied during 1962–2001 in few parts of the Zanskar valley, western Himalaya indicated an area loss of 18.2% with the snout retreat rate varying from 6 to 33 m a^{-1} (Nathawat et al., 2008). In a recent study over the Kashmir Himalayan region, located in western Himalaya, Murtaza and Romshoo, (2015) reported a 17% loss in area of glaciers. In Zanskar Himalayan Range, (Pandey et al., 2011) has noted a terminus retreat rate of 3–42 m a^{-1} and up to 88 m a^{-1} of 26 glaciers during the period from 1975–1989 and 1989–2001 respectively. A similar study, carried out by Nathawat et al., (2008) in the parts of Doda Valley, Zanskar mountain range reported a retreat rate of 6–33 ma^{-1} between the years 1962-2001 based on analysis of 13 glaciers. In the same region, Kamp et al., (2011) in a current study, reported a retreat rate of 23 ma^{-1} and 10–55 ma^{-1} during 1975–2003 and 2003–2008 respectively). In the

Himalayan region, the retreat of glaciers will have a large impact, as glaciers play an important role in river runoff (Huss and Hock, 2018).

In the Himachal Himalaya, Northwest Himalayan region, the glaciers considered during the years from 1962-2001 in the Chenab basin has retreated at a rate of 0.53% a^{-1}, in Parbati at a rate of 0.56% a^{-1} and in Baspa at rate 0.48% a^{-1} (Kulkarni et al., 2007). In the Chenab Basin, the Samudra tapu glacier's snout has receded by about 756 m during 1963–2004 and the total glacier area was reduced by 13.7 km^2 (Shukla et al., 2009). Temporal variability is observed in the Gangotri Glacier, a well-monitored Indian glacier, (Kargel et al., 2011). In Khumbu Himalaya, an average glacier area loss of about 5% has been reported between the years 1962-2005 (Bolch et al., 2008). A 19% glacier loss is reported in Warwan basin western Himalaya (Brahmbhatt et al., 2012) during 1962–2001. Similarly, the glaciers in the Central Himalaya are maintaining a continuous trend of retreat over the past few decades with an average retreat rate of 5.5–8.7 ma^{-1} (Ren et al., 2004, 2006). In the Indian Himalaya, studies on snout recession/mass balance carried out on a few glaciers have revealed generally a negative trend (e.g., Kulkarni, 2007; Kumar et al., 2007; Wagnon et al., 2007; Dobhal et al., 2007; Pithan, 2011; Berthier, et al., 2007; Bolch et al., 2011; Mir et al., 2013b). During last decades, the aggregate mass balance of Himalayan glaciers has been reported negative (Ren et al., 2006) with the exceptions of glaciers in higher Karakoram mountain range (Hewitt, 2005). The field measurements of glacier mass-balance have been carried out on few glaciers, such as Dokriani Glacier (1992–1995,1997–2000 and 2007–present) and Chorabari Glacier (2003–present) in the Garhwal Himalaya (Dobhal, 2009; Dobhal and Mehta, 2010) Chhota Shigri Glacier in Himachal Himalaya and Hamtah glacier in Spiti basin (Wagnon et al., 2007). The overall mass balance of Chhota Shigri glacier is about -0.67 mwe a^{-1}, Dokriani glacier is -0.32 mwe a^{-1} and that of Hamtah glacier is -1.60 mwe a^{-1} (Dobhal and Mehta, 2010). Based on satellite data, Kulkarni et al., (2011) reported recently glacier loss of about 1868 glaciers studied in 11 basins

of the Indian Himalaya. They reported an overall reduction in glacier area of 16% ranging from 2.7-20% among different basins studied during 1962-2002 (Figure 3). The changes in glacier areas are also likely to influence the runoff trends in the 21st century i.e. runoff could increase in the initial decades and then decrease or cease due to substantial decrease in glacier area (Bliss et al., 2014; Lutzet al., 2014; Bolch et al., 2012).

Depending upon the topographic and other local factors of the glaciers, a heterogeneous pattern of glacier loss in different areas and basins of the Himalayan region has been reported; and thereby, understanding the influence of the local factors on glacier changes has received an ample attention during last year's (Basnett et al., 2013; Thakuri et al., 2014). Among the various notable factors, the glacier size, debris cover and topographic variables (altitude, slope, and aspect) are the most important variables in determining the variable rates of glacier changes. A number of earlier studies have found an inverse relationship between the glacier size and rates of loss (e.g., Kulkarni et al., 2007; Mark and Seltzer, 2005; Chueca et al., 2007, Mir et al., 2013a). In other words, the smaller glaciers have experience generally higher rates of loss than large glaciers. A similar pattern has been reported from Garhwal (Bhambri et al., 2011) and Himachal Himalaya (Deota et al., 2011) recently. The tendency of larger glaciers to less loss has also been reported by many other studies (e.g., Racoviteanu et al., 2008a; Salerno et al., 2008; Loiblet al., 2014). In general, a loss of 38% of small glaciers (<1 km^2) and 12% of larger glaciers has been reported In Western Himalaya between 1962–2001 by a study carried out by Kulkarni et al., (2005). Similarly, the higher elevations of glaciers significantly reduce the rates of glacier loss (Kulkani et al., 2007; Racoviteanu et al., 2008). The glaciers with a smaller altitudinal range along with median altitudes closer (in altitude) to their maximum altitudes are losing more of their area (Ye et al., 2003; Mark and Seltzer, 2005). The glaciers slope is another topographic variable and plays a significant role in determining glacier changes i.e., the steeper the glacier, the larger the loss. The similar influence of slope on glacier has

been observed from the Khumbu area (Salerno et al., 2008; Racoviteanu et al., 2015). The orientation or the aspect of the glaciers significantly controls the glacier changes. The glaciers losing maximum area are generally oriented southwards and southwest (Salerno et al., 2008, Bhambri et al., 2011; Mir et al., 2013a). The similar patterns have been reported from the Alaknanda and Tirungkhad basins (Nainwal et al., 2008b; Mir et al., 2013b). Furthermore, the presence of supra-glacial debris cover has a dominant effect on the glacier loss. The debris cover with thickness exceeding a few centimeters leads to a considerable reduction in glacier loss (Mattson et al., 1993; Scherler et al., 2011). The glaciers which are heavily covered with a thick debris cover respond more slowly to climatic changes than glaciers with thinner debris cover or clean glaciers (Singh et al., 2000; Scherler et al., 2011). I addition, the debris cover is also an important factor for mass balance and glacier dynamics because the debris thickness determines the ice melt rate (Mattson et al., 1993; Zhang et al., 2011). In the Himalayan region, the glacier shrinkage and mass loss has been recognized concurrently with an increase in debris cover (Bolch et al., 2011; Nuimura et al., 2012).

Similarly, there are several regional as well as global studies on long term snow cover changes (e.g., Brown, 2000; Beniston et al., 2003; Laternser and Schneeneli, 2003; Kazuyuki, 2003; Bednorz, 2004). Significant reductions in snow depth have been reported in western Canada (Brown, 1996 & 1998). In another study, Ke et al., (2009) observed trends in snowfall in Qinghai, China. In the northern Hemisphere, the snow cover variation and its relationship to temperature have been studied by Frei and Robinson, (1999). Similarly, Dickson, (1984) and Clark et al., (1999) have studied and reported the climatic effect of Eurasian snow cover variations on the Indian monsoon rainfall. Similarly, the significant recent changes in glacial and snow cover extent are reported from different parts of Himalayan region too (e.g., Niederer et al., 2008; Nie et al., 2010, Kulkarni et al., 2010; Mir et al., 2013a). Mir et al., (2014) has studied snowfall variability in response to temperature in Satluj Basin, Western Himalaya,

India. The changes in snow cover and glaciers are mostly attributed to changing pattern of snowfall and temperature (Shekhar et al., 2010; Mir et al., 2013b). Mir et al., (2015b) suggested that the insignificant decline in snowfall has resulted in a significant decline in snow covered area (SCA) studied between the years from 2000-2009 in the Satluj basin. Thus, the variations in snow cover are also considered and cited as useful indicators of climatic fluctuations (Barry, 1985; Chang et al., 1990; Goodison and Walker, 1993; Derksen et al., 2000; Serreze et al., 2000).

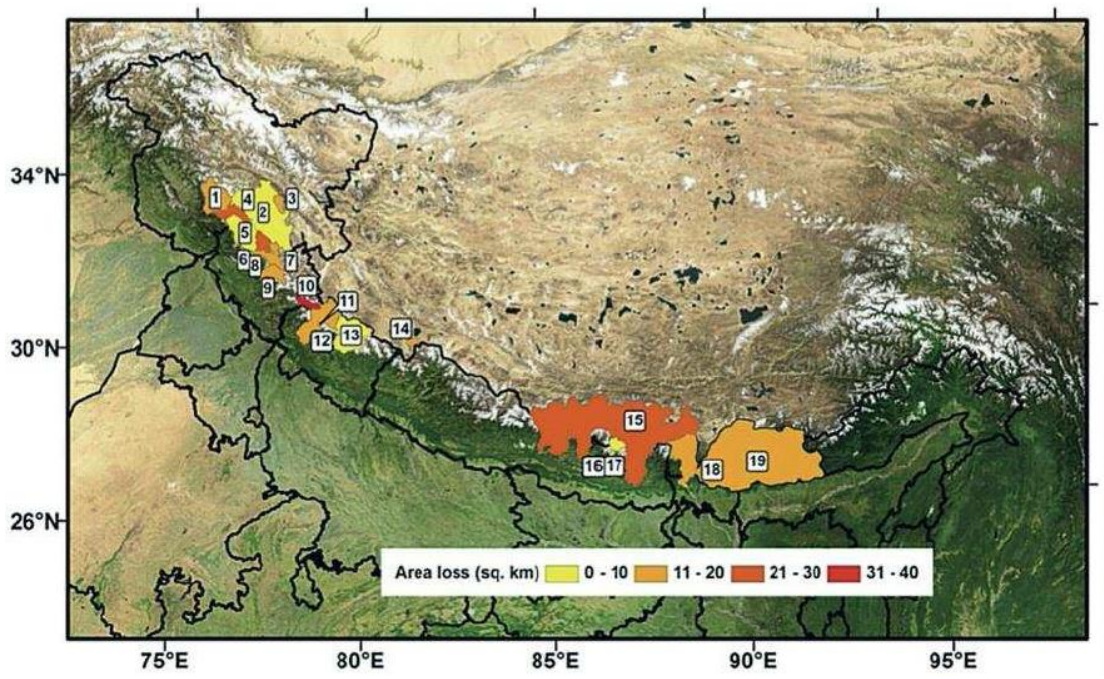

Figure 2: Map showing the loss in glaciers (%) within different basin of the Himalaya region from 1960-2000, based on satellite images. The various sub-basins include 1. Bhut, 2. Zansker, 3. Kang Yatz Massif, 4. Warwan, 5. Miyar, 6. Bhaga, 7. SamudraTapu, 8. Chandra, 9. Parbati, 10. Baspa, 11. Bokriani, 12. Bhagirathi, 13. Alaknanda, 14. Naimona'nyi region, 15. Mt. Everest region, 16. AX010, 17. Sagarmath national partk, 18. Tista, 19. Bhutan Himalaya (source: Kulkarni, 2011).

3.2 Climatic fluctuations

An analysis of the temperature data over the Himalayan region has immensely revealed a warming pattern, albeit at diverse rates during different periods depending on the seasons and

regions. In the tune of the other regions (Reda et al., 2013a, b; Diodato et al., 2011), recently Brohan et al., (2006), using Climate Research Unit's (CRU) reconstructed temperature dataset; reported a higher rate of warming in the Himalayan and Tibetan Plateau regions during last few decades. For example, Brohan et al., (2006), observed a warming of 0.5 °C in annual average maximum temperature (T_{max}) during 1971-2005 as compared to a lower warming during 1901-1960. Similarly, another study by Dash et al., (2007) in the Indian western Himalaya reported a warming and rise of 0.9 °C over a study period of 102 years (1901-2003). Dimri and Dash, (2011) also reported a rising pattern in temperature over the western Indian Himalaya. They reported a greatest increase in T_{max} (1.1 to 2.5 °C) using the winter (December to February) monthly temperature data from 1975-2006. In the northwest Indian Himalayan region, Bhutiyani et al., (2007) have observed a 1.6 °C rising pattern (0.16° C /decade) during last century. In the northwest Indian Himalayan region over the lower Indus basin, Singh et al., (2008), found increasing trends in T_{max} and seasonal average of daily T_{max} for all seasons except monsoon. In addition, the trends of seasonal and monthly mean temperatures between the years 1994-2003 indicated a shift in the peak summer and winter seasons in the Northwestern Himalaya (Koul and Ganjoo, 2010). Mir et al., (2015a, b) reported an increasing trend in temperature, particularly a significant rise in T_{min} from 1983-2008 in Indian part of Satluj basin located in western Himalaya. Similar, in another study, increasing trends of the winter T_{max} studied over upper Indus basin has been also reported by Khattak et al., (2011). In general, an increase of 1.0 and 3.4°C in T_{max} and T_{min} studied over a period from the years 1988-2008over the Himalayan region has been reported by (Shekhar, 2010). An analysis of temperature data over the Nepalese Himalaya also witnessed a warming pattern during last century (Shrestha et al., 1999). Similarly, the Everest (Qomolangma) region in China also exhibit warming pattern at an average rate of 0.234 °C/decade in T_{avg} between the years 1971-2004 (Yang et al., 2006). Importantly, the rate of warming pattern reported; is observed to be constantly higher during

winter season than other seasons in most parts of the Himalayan region such as the Chinese, northwest Indian, and Nepalese Himalaya (Bhutiyani et al., 2010; Shrestha and Devkota, 2010; Mir et al., 2015a). Thus, later quarters of the 21st century and recent decades are recognized to be warmer than earlier periods along with the warming rate higher in winter season than other seasons across the region.

Contrary to warming pattern, the precipitation in the Himalayan region lacks the spatially consistent long-term trends. In a recent study, Recently, Bhutiyani et al., (2010) based on analysis of data of three stations, suggested a statistically significant negative trend (at 5% significance level) in monsoon and average annual rainfall assessed from 1866-2006 in the Indian northwest Himalayan region. A similar but insignificant negative pattern is reported for a period from 1960-2006 over the Western Indian Himalaya region (Sontakke et al., 2009). Dimri and Dash, (2011) recognized a significant decline in winter precipitation (December-February) in the Himalayan region during 1975-2006 and the pattern lacked spatially consistent phases among stations. During 1901-2003, Guhathakurta and Rajeevan, (2008) also reported a significant downward pattern in winter precipitation over the states of Jammu & Kashmir and Uttarakhand. Similarly, an insignificant declining trend has been reported from the years 1970-2008 in snowfall with a week rising trend in rainfall in the Satluj basin, western Himalaya (Mir et al., 2015a). Mir et al., (2015a, b &c) reported the decline in snowfall in response to rising temperature, particularly T_{min}. They suggested that the insignificant decline in snowfall has resulted in a significant decline in snow covered area (SCA) studied between the years 2000-2009 in the basin. However, during 1961-1999 in the upper Indus Basin (Pakistan), statistically significant increasing trends are observed in winter precipitation (Archer and Fowler, 2004; Fowler and Archer, 2005), but no trend is observed during the longer period considered in the study (1895-1999). Interestingly in the Himalayan region, Dimri and Dash, (2010, 2012) and Shekhar, (2010) have reported that the negative trends in the precipitation are associated with

a reduction in total seasonal snowfall. The increase in temperature is one of the important factors responsible for reduction in snowfall (Thayyen et al., 2005; Dimri et al., 2007). In the Bhutan Himalayan region, previous reports on the precipitation trends have suggested largely random fluctuations and the absence of trend on annual or seasonal basis (Tse-ring, 2008). Similarly, Shrestha et al., (2000) did not find any significant long-term trends in precipitation data (1959-1994) of the Nepalese Himalaya. In general, the precipitation is decreasing in the Western Indian Himalaya with the decline in winter precipitation as well but with intra-regional differences.

The changes in stream flow pattern are generally dependent on the land use and climate changes. While observing the stream flow pattern of river in northwestern Indian Himalayan region during last three decades, Bhutiyani et al., (2007) reported a significant rise in the number of high-magnitude flood events in the area. Mir et al., (2015a) reported a continuous and significant decline in stream flow of Satluj river basin located in western Himalaya between the years 1963-2008. Similarly, Khattak et al., (2011) has reported an increasing trend in the winter and spring stream flow pattern in the upper Indus Basin, Pakistan. However, it is important to note that the Nepalese stream flow trends showed ambiguous spatial patterns studied during 1965-1995 (Gautam and Acharya, 2012). Over the Tibetan Plateau, Yao et al., (2007) found an up rise of 5.5% in river runoff and attributed it to the glacial melting. Similarly, Jasrotia et al., (2013) assessed the impact of climate change on the hydrological regime of Chenab basin, Western Himalaya and reported a declining pattern. In the northwestern Himalaya, based on the trend analysis of discharge data of rivers for the period between the years 1922–2004, Bhutiyani et al., (2008) related the negative discharge trends during winter and monsoon seasons in the post 1990 period with the falling contribution of glaciers to the discharge and their gradual disappearance. In response to warming temperatures, the increased contribution to stream flow of glacial and snowmelt are noted as causes for the upward trend

in stream flow in low flow periods and in areas of low precipitation e.g. Tibetan Plateau and Indus basin (Mukhopadhyay, 2014; Mukhopadhyay et al., 2014). Similarly, over the northwestern Himalayan region, Fowler and Archer, (2006) analyzed temperature data during the period between the years 1961-2000 and connected a decrease of 20% in summer runoff in the rivers Shyok and Hunza to the observed 18°C drop in mean summer temperature since 1961 and growth of Karakoram Glacier.

Time series analysis of observational records (Burger et al., 2018) is a useful tool to establish general data trends but is of limited use when observations are scarce in space and time and cannot provide insights into which processes drive observed changes. Additionally, while satellite-based glacier inventories (Barcaza et al., 2017; Malmros et al., 2016; Falaschi et al., 2013) aided the establishment of baseline areal changes, they do not generally assess mass balance or volumes change and cannot be used to explain the causes of observed changes. Therefore, there is a need for an integrated approach to understand the midterm and long-term changes in glaciers and glacier runoff in the high-elevation catchments of the Himalayan region.

Keeping in view the above concern, our main aims are to estimate the corresponding glacier contribution to runoff and impact assessment of snow/glacier change on runoff in the recent past. These aims are addressed through application of a physically oriented and fully distributed glacio-hydrological model, in situ data, and glacier change estimates for a basin located in Western Himalaya. Therefore, in this study, SPHY model has been simulated in two times: (i) 2003-2010 and (ii) 2011-2018 utilizing variable degree-day factors to highlight the effect of snow and glacier changes on runoff.

CHAPTER 4

METHODOLOGY

4.1 Snow covered areas and glacier mapping

For snow mapping, MODIS (MOD10A2) 8-daily satellite derived snow cover areas have been utilized for the year 2003-2018. The MOD10A2 snow cover data products contain data fields for maximum snow cover extent over an eight-day compositing period. The MODIS (MOD10A2) consists of 1200 km by 1200 km tiles that employs a Normalized Difference Snow Index (NDSI) and other criteria tests (Shukla et al., 2017) (Figure 4). To highlight the elevation wise similarities in the distribution of snow covers, the fractional snow cover corresponding to multiple elevation zones were computed on the monthly scale for both SPHY derived snow covers and MODIS derived snow covers. Shukla et al. (2017) carried out a study for Satluj basin in which all the maps were generated. The snow cover areas maps for Baspa basin have been extracted from these maps. Therefore, the 8-daily scenes of MODIS snow cover were aggregated at monthly scales to compare with the SPHY derived snow covers.

As per the study of Mir et al. (2017), number of glaciers were mapped in the Baspa basin for years 1966, 1999, 2000 and 2000. In this study, Landsat data series-based satellite scenes have been utilized for the year 2018. For the Landsat 8, ETM+ and TM data images, the glaciers were delimited using band ratios of near infrared and shortwave infrared bands (Singh and Goyal, 2018; Shukla et al., 2010). The debris free glacier (or clean-ice glacier) mask was generated in the binary image utilizing threshold values between 2.2 to 2.5. Several misclassified glacier areas were eliminated by post-processing of the data. Finally, the glacier images were converted from binary to vector data layers. The detail glacier mapping methodology has been employed previously by Mir et al. (2017). To find out the glacier changes corresponding to each elevation zone, the spatial analyst module of ArcGIS was

utilized. To find out the correlation between glacier changes and corresponding elevation, the variation in glaciers was highlighted with respect to elevation in the progressive manner from 2000 to 2018. The changes in glaciers with respect to elevation have been analyzed to highlight the elevation dependent warming and its impact on glacier mass changes.

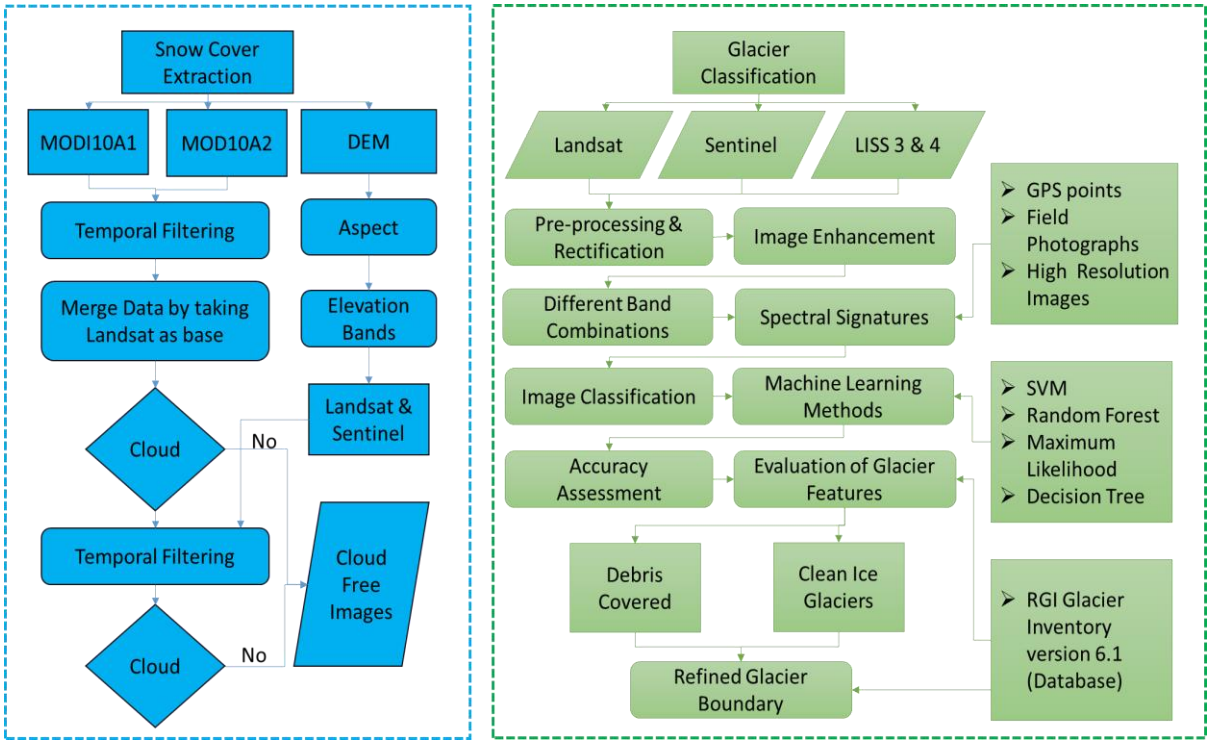

Figure 3: Showing the computation methodology of snow cover and glacier maps.

4.2. Snowmelt and glacier melt hydrology of SPHY Model

SPHY is a spatially distributed and can be applied on a grid-by-grid basis (Terink et al., 2015). SPHY works in a python-based environment using PC Raster and its source codes are freely available (*http://www.sphy.nl/*). In SPHY, each grid value is represented average over the grid. In SPHY model, for glaciers, a sub-grid variability exists, and a grid can be defined as glacier free, completely covered by glacier or partially covered by glacier. The glacier free grid/fraction of grid can be defined as snow covered or snow free. The grid/area which is free from snow can be defined by vegetation, open water, and bare soil (Terink et al., 2015). The

soil column structure of SPHY model is quite similar to VIC model (Terink et al., 2015), including two upper soil and third groundwater storages. The three drainage components; surface runoff, lateral flow and baseflow can be defined in SPHY model. SPHY computes i.e. each grid precipitation in the form of snow or rain, depending on the defined critical temperature value.

Precipitation that falls on the ground can be intercepted by vegetation and some amount or whole can be evaporated. In SPYHY, the snow storage is updated with snow accumulation and/or snowmelt. Surface runoff is a part of liquid precipitation, whereas the rest infiltrates into the soil. In SPHY, the resulting soil moisture is subject to evapotranspiration (ET), which is depended on the soil properties and fractional vegetation cover, whereas the rest contributes to streamflow (or discharge) by means of the baseflow resulting from the groundwater zone and lateral flow from the first soil layer. In SPHY, the modified Hargreaves equation that is a function of temperature only has been used for the ET computation (Terink et al., 2015). As per the earlier studies, it was observed that Hargreaves method performed well over Himalaya, while in the absence of large amount of the datasets (Singh and Goyal, 2017; Arnold et al., 2012). The grid-specific runoff that is available for routing, can be contributed by surface runoff, lateral flow, baseflow, snowmelt and glacier melt.

SPHY model requires physical/thematic data inputs such as digital elevation model (DEM), landuse/lancdcover (LULC) map, glacier map highlighting clean ice glaciers and debris glaciers, soil parameters such as root depth, maximum capillary rise, seepage, groundwater parameters such as baseflow, groundwater depth, aquifer yield. The meteorological datasets such as temperature, precipitation, radiation is minimally required to setup the model. The snow-covered area (SCA) can be utilized for the validation of SPHY generated snow cover. The SPHY model provides all watershed components such as total

runoff, snowmelt runoff, baseflow, ET, groundwater runoff, groundwater level, glacier melt runoff, and rainfall-runoff in daily, monthly, and annual basis (Terink et al., 2015).

This study mainly explores the snow and glacier melt runoff characteristics of the selected Baspa River Himalayan basin and therefore, the focus of this study has been given to the processes and parameters relevant to the snow and glacier hydrology. The equations of the other components and processes are previously discussed in detailed Terink et al. (2009). The snow-glacier melt runoff hydrology has been described below in further sections.

4.2.1 Snowfall and rainfall

In SPHY, the dynamic snowfall mass balancing can be performed at a daily time step. Using a temperature threshold, the falling precipitation can be defined as a snowfall (solid form) and rain (liquid form). The snow accumulation (or snowpack or snowfall) can be calculated as (eq. 1):

$$P_{s,t} = \begin{Bmatrix} P_{et}\ if\ T_{avg,t} \leq T_{crit} \\ 0\ if\ T_{avg,t} > T_{crit} \end{Bmatrix} \quad \text{.....(1)}$$

Where, $P_{s,t}$ (mm) is the snowfall on the day *t*, P_{et} (mm) can be defined as the effective precipitation on day t, $T_{avg,t}$ (◦C) is the mean air temperature on day *t*, and T_{crit} (°C) is a calibrated temperature threshold for precipitation to fall as snow. Whereas, the precipitation falls as liquid precipitation can be computed as (eq. 2):

$$P_{l,t}(liquid\ precipitation) = \begin{Bmatrix} P_{et}\ if\ T_{avg,t} > T_{crit} \\ 0\ if\ T_{avg,t} \leq T_{crit} \end{Bmatrix} \text{.....(2)}$$

4.2.2 Snowmelt storage and runoff

SPHY model uses a degree-day approach using temperature index model for the calculation of snowmelt (Terink et al., 2015). The application of degree-day models is

widespread in cryospheric models that is based on an empirical relationship between melt rate and air temperature (Terink et al., 2015). Based on the degree-day approach, the potential snowmelt can be calculated as (eq. 3):

$$A_{pot,t} = \begin{cases} T_{avg,t} * DDF_s & if\ T_{avg,t} > 0 \\ 0 & if\ T_{avg,t} \leq 0 \end{cases} \ldots..(3)$$

with $A_{pot,t}$ (mm) is defined as the potential snowmelt on day t, and DDFs (mm°C^{-1} day^{-1}) is denoted as a calibrated degree-day factor for snow. The actual snowmelt can be limited by the snow storage at the end of the previous day, and is computed as (eq. 4):

$$A_{act,t} = min\left(A_{pot,t}, SS_{t-1}\right) \ldots..(4)$$

Here, $A_{act,t}$ (mm) is defined as the actual snowmelt on day t, and SS_{t-1} (mm) is denoted as the snow storage on day $t-1$. After that the snow storage from day $t-1$ is updated to the present day t, utilizing the actual snowmelt ($A_{act,t}$) and the solid precipitation ($P_{s,t}$). When temperature falls below the melting point, then the meltwater (that is frozen) in the snowpack during time $t-1$ will be added to the snow storage as (eq. 5):

$$SS_t = \begin{cases} SS_{t-1} + P_{s,t} + SSW_{t-1} & if\ T_{avg,t} < 0 \\ SS_{t-1} + P_{s,t} - A_{act,t} & if\ T_{avg,t} \geq 0 \end{cases} \ldots..(5)$$

Here, SS_t is defined as the snow storage on day t, SS_{t-1} is described as the snow storage on day $t-1$, $P_{s,t}$ is the solid precipitation on day t, $A_{act,t}$ is the actual snowmelt on day t, and SSW_{t-1} is the amount of frozen meltwater on day $t-1$. The units for all terms are mm. The maximum of meltwater that can freeze (SSWmax (mm)) is thus limited by the thickness of the snow storage (Terink et al., 2015). The total snow storage (SST(mm)) consists of the snow storage and the freeze meltwater can be calculated as (eq. 6):

$$SST_t = (SS_t + SSW_t) \times (1 - GlacF) \ldots..(6)$$

Where, $(1 - GlacF)$ is defined as the fractional grid that is not covered by glaciers. In SPHY model, snow melt and snow accumulation can only be calculated when grid fraction determined as the land surface. In SPHY, the runoff from snow (SRo (mm)) can be calculated when the air temperature reaches above the melting point (Terink et al., 2015). The change in meltwater stored in the snow can be accounted as (eq. 7):

$$\Delta SSW = SSW_t - SSW_{t-1} \text{ .....(7)}$$

4.2.3 Glacier process and runoff

In SPHY, glaciers are considered melting surfaces which can partly or completely cover the grid cell. Glacier melt is also calculated by the degree-day approach and the melt rates of debris covered and debris free glaciers vary (Terink et al., 2015). The melt from the debris free glaciers can be computed as (eq. 8):

$$A_{CI,t} = \begin{cases} T_{avg,t} \times DDF_{CI} \times F_{CI} & if\ T_{avg,t} > 0 \\ 0 & if\ T_{avg,t} \leq 0 \end{cases} \text{.....(8)}$$

Where, DDF_{CI} (mm $^{O}C^{-1}$ day^{-1}) is a degree-day factor for debris free glaciers and can be calibrated for the given area/grid. F_{CI} $(-)$ is the fraction of debris-free glaciers within a grid. The daily melt from the debris-covered glaciers can be calculated as (eq. 9):

$$A_{DC,t} = \begin{cases} T_{avg,t} \times DDF_{DC} \times F_{DC} & if\ T_{avg,t} > 0 \\ 0 & if\ T_{avg,t} \leq 0 \end{cases} \text{.....(9)}$$

Where, DDF_{DC} (mm $^{O}C^{-1}$ day^{-1}) is a degree-day factor for debris-covered glaciers and can be calibrated for the given area/grid. F_{DC} $(-)$ is the fraction of debris-covered glaciers within a grid. The total glacier melt, $A_{GLAC,t}$ (i.e. summing the melt water from debris-free and debris-covered glaciers) can be accounted as (eq. 10):

$$A_{GLAC,t} = \left(A_{CI,t} + A_{DC,t}\right) \times GlacF \text{.....(10)}$$

From the total melt from glaciers, a fraction of the glacier melt percolates to the groundwater and the remaining fractions run off. Finally, the generated runoff GRo (mm) from glacier melt is defined as (eq. 11):

$$GR_{ot} = A_{GLAC,t} \times (1 - GlacROF) \text{.....(eq. 11)}$$

4.2.4 Surface runoff, total runoff, and routing

In SPHY, soil water processes can be determined by the three soil layers such as root zone, sub zone and groundwater layer. The equations related to soil processes are previously described by Terink et al. (2009) and therefore not discussed in detail. SPHY is a water-balance model and therefore the SPHY only accounts for stresses regarding water shortage and water excess. SPHY uses an ET reduction parameter ($ETred_{wet}$) that has 0 value in soil saturated condition and otherwise 1 (Terink et al., 2015). SPHY uses the saturation excess overland flow process (i.e. Hewlettian runoff) to compute the surface runoff (RO) (Terink et al., 2015) as (eq. 12):

$$RO = \begin{cases} SW_1 - SW_{1,sat} & if\ SW_1 > SW_{1,sat} \\ 0 & if\ SW_1 \leq SW_{1,sat} \end{cases} \text{.....(12)}$$

Here, SW_1 (mm) is the water content in the first soil layer and $SW_{1,sat}$ (mm) is defined as the saturated water content of the first soil layer. In SPHY, the exceeded water from the field capacity has been used for lateral flow (Terink et al., 2015). SPHY assumes the lateral flow travel time to be dependent on the field capacity, saturated conductivity, and saturated content (Terink et al., 2015).

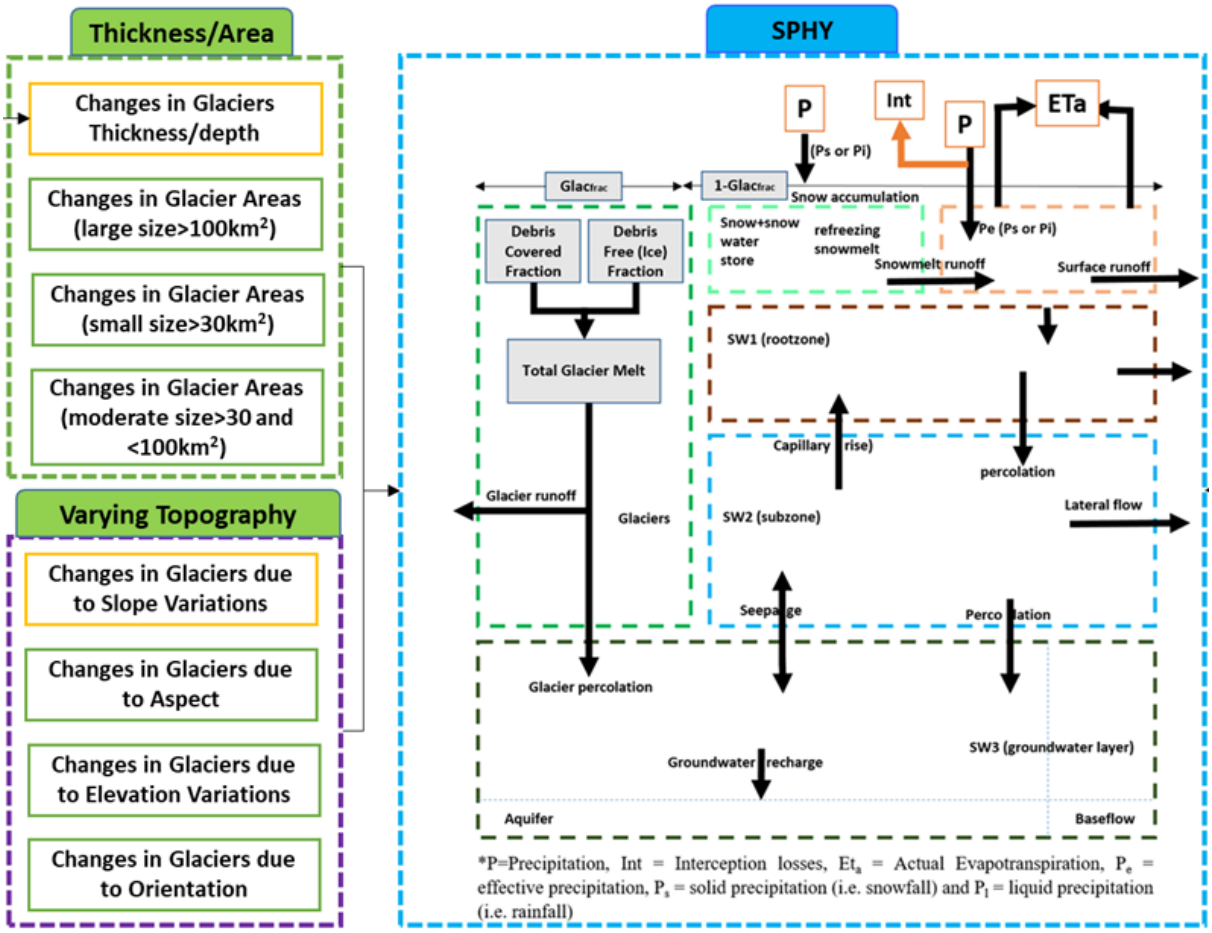

Figure 4: Schematic and methods of SPHY modeling framework.

In SPHY, water can percolate from the first soil layer to the second soil layer, and from the second to the third soil layer. In SPHY, water only percolates when the water content will exceed the field capacity of that layer (Terink et al., 2016). SPHY utilizes exponential decay weighting function (Terink et al., 2015) in the precipitation groundwater response model similar to SWAT model (Arnold et al., 2012). For baseflow computation, SPHY uses steady-state response of groundwater flow and water table fluctuations which can be resulted by the non-steady response of the groundwater flow (Arnold et al., 2012). In this model, baseflow can only be occurred when the amount of water stored in the third soil layer exceeds a certain threshold. For runoff routing, SPHY computes for each grid the accumulated amount of water that flows out of the grid into its neighbouring downstream grid through the accuflux PCRaster

built-in function, which computes runoff at each grid from its upstream grids and also adding the runoff amount that is generated within the grid itself (Terink et al., 2015) (Figure 5).

4.3. Model Calibration

In SPHY, both manual and auto-calibration can be performed. In this study, mostly real time, observed and measured datasets and other parameters/coefficients have been used. To get the practical parametric response, the manual calibration based on trial-and-error basis was preferred. Sometimes, it has been seen that the auto calibration does not give the reliable estimates of modeling parameters when large numbers of parameters are involved (Terink et al., 2015). During modeling, the best fitted value of the parameter has been calculated as per trial-and-error method. The observed daily discharge is available from 2003 to 2018 and thus utilized for the present study. For manual calibration, parameters such as temperature threshold to fall as snow (Tcrit), degree-day factor for snow (DDFs), glacier fraction of grid cell (GlacF), degree-day factor for debris-free glaciers (DDF_{CI}), degree-day factor for debris-covered glaciers (DDF_{DC}), and threshold for baseflow to occur (BF_{thres}) have been taken into consideration.

MODIS based snow cover area have been extracted to compare the SPHY derived snow cover on the monthly scale for the year 2010 and 2018 so that snow parameters required to run the model, which can be accurately defined in the model and modeling accuracy can be improved. In this study, the real time digitized glacier maps, characterizing by debris-free glaciers and debris-covered glaciers, were used to define the glacier properties over the basin. Other parameters (e.g. related to soil and LULC) values are set based on the literature survey (Terink et al., 2015) and standard global values suggested by SPHY model (Terink et al., 2015), which have been developed specifically for the Himalayan conditions.

Utilizing large number of datasets and parameters as an input to the SPHY model, the model has been setup for the two-time durations (i.e. 2003-2010 and 2011-2018) to understand the snow melt and glacier melt runoff variations. The SPHY model was simulated at the daily time step at 250 m spatial resolution scale and SPHY re-gridded all data inputs at the same scale (Terink et al., 2015). However, the modeling variables can be computed on a daily, monthly, and yearly scales, as per the user's choice. The modeling outcomes have been evaluated at the outlet and site scale.

Table 3: SPHY model parameters used for the simulation during both time series i.e. 2003-2010 and 2011-2018.

SI. No.	**Name of the Parameter**	**Description (Unit)**	**Parameer Ranges (min-max)**	**Fitted Value**
1	RootDepthFlat	Rootzone depth (mm)	300-1000	500
2	SubDepthFlat	Thickness of subsoil (mm)	1000-2000	1500
3	CapRiseMax	Maximum capillary rise from subsoil to rootzone (mm/day)	2 to 10	5
4	GwDepth	Thickness of groundwater layer (mm)	1000-4000	3000
5	GwSat	Saturated water content in groundwater zone (mm)	500-3000	2000
6	alphaGw	Baseflow groundwater range	0.1-1.0	0.05
7	DDFG	Glacier clean ice degree-day factor (mm degree-1 day-1)	2.0-8.0	5.5
8	DDFDG	Glacier debris degree-day factor (mm degree-1 day-1)	2.0-8.0	5.0
9	Tcrit	Critical temperature for precipitation to fall as snow (degrees Celsius)	-0.5-5.0	3.0
10	DDFS	Snow degree-day factor (mm degree-1 day-1)	2.0-8.0	6.0
11	kx	Recession coefficient of routing (-)	0.5-1.0	0.95

Note: The parameters ranges (min-max) used in the above Table 3 have been selected based on the standard values as suggested by SPHY and literature survey.

4.4 Snowmelt glacier melt and glacier area changes

For analyzing the changes in snowmelt and glacier melt runoff, the whole time series (2003-2018) was divided in two-time series (TS) sets: (i) TS1 2003-2010 and (ii) TS2 2011-2018. The main purpose of the dividing time series sets in two durations was to analyze the effect varying climate conditions (such as temperature and precipitation variations) along with observed glacier mass changes on the resultant glacier melt runoff. As per the comparison of both period glacier maps (i.e. 2000 and 2011), a significant mass reduction was observed. Therefore, while setup the SPHY for the TS1 (i.e. 2003-2010), the glacier map prepared for the year 2000 was utilized; whereas, during TS2 setup in SPHY, the glacier map prepared for the year 2011 was utilized. The changes in glacier mass are compared to the corresponding elevations to find out the elevation dependent warming and their impacts on glacier and glacier melt runoff changes. A very few studies highlighted that temperature and precipitation is highly varying over Himalaya and showed the elevation dependent warming, especially in last 20 years they recorded the maximum variations (Shukla and Goyal, 2020; Rem et al., 2017; Singh and Goyal, 2016).

The main water balance components such as simulated runoff (Q, mm), rain Q (mm), snow Q (mm) and glacier Q (mm) have been computed at the outlet (i.e. Sangla gauge). Small watersheds considering 30 sites (shown in Figure 1) on the main stream and tributaries were created. Out of 30 sites, 17 independent sites located on the tributaries were chosen dominated by snow and glaciers, which have been used to explore the snow melt and glacier melt runoff variation. Glaciers are situated at the extreme high elevation zones, whereas non-glaciated areas covered by snow situated at the moderate elevation zones. These snow melt and glacier melt changes have been analyzed on the monthly, seasonal, and annual basis during both durations (e.g. 2003-2010 and 2011-2018). In addition to glacier maps of 2000 and 2011 used for the period of TS1 and TS2, 2018 glacier map has also been used for TS2.

CHAPTER 5

RESULTS AND DISCUSSION

5.1 Snow and glacier mapping

On the basis of glacier maps, a significant reduction has been computed in the glacier areas from 2000 to 2018 (Fig. 5). A significant variation in snow covered areas (SCAs) observed by previous studies (Shukla et al., 2017; Mir et al., 2017), have identified in different portions of the basin. Therefore, to highlight the effect of these snow and glacier areas variations, different glacier maps (e.g. 2000, 2006, 2011 and 2018) were used so the effect of glacier areas reduction can be easily incorporated in the modeling outcomes.

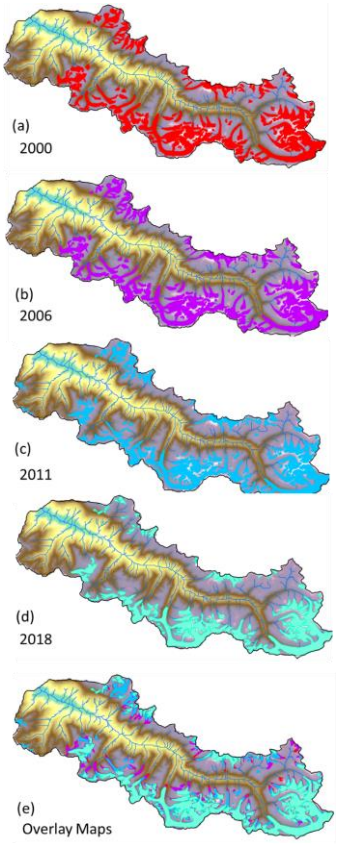

Figure 5: Temporal variations in glacier maps of Baspa basin highlighting reduction in the glacier area from 2000 to 2018: (a) 2000, (b) 2006, (c) 2011, (d) 2018 and (e) overlay of all year maps.

The accuracy of SPHY derived snow covers has been tested with reference to the MODIS derived snow covers for the year 2010 and 2018 (Figs. 6, 7 and 8). The visual comparison of SPHY and MODIS derived snow-covered areas (SCA) can be seen in Fig. 6. In Fig. 6, based on the monthly plots one can see that most of months have shown similar pattern of SCA when compared to SPHY and MODIS SCAs for both time series durations. However, during May and June months, some inconsistency in SCA can be seen when compared both datasets (Fig. 6).

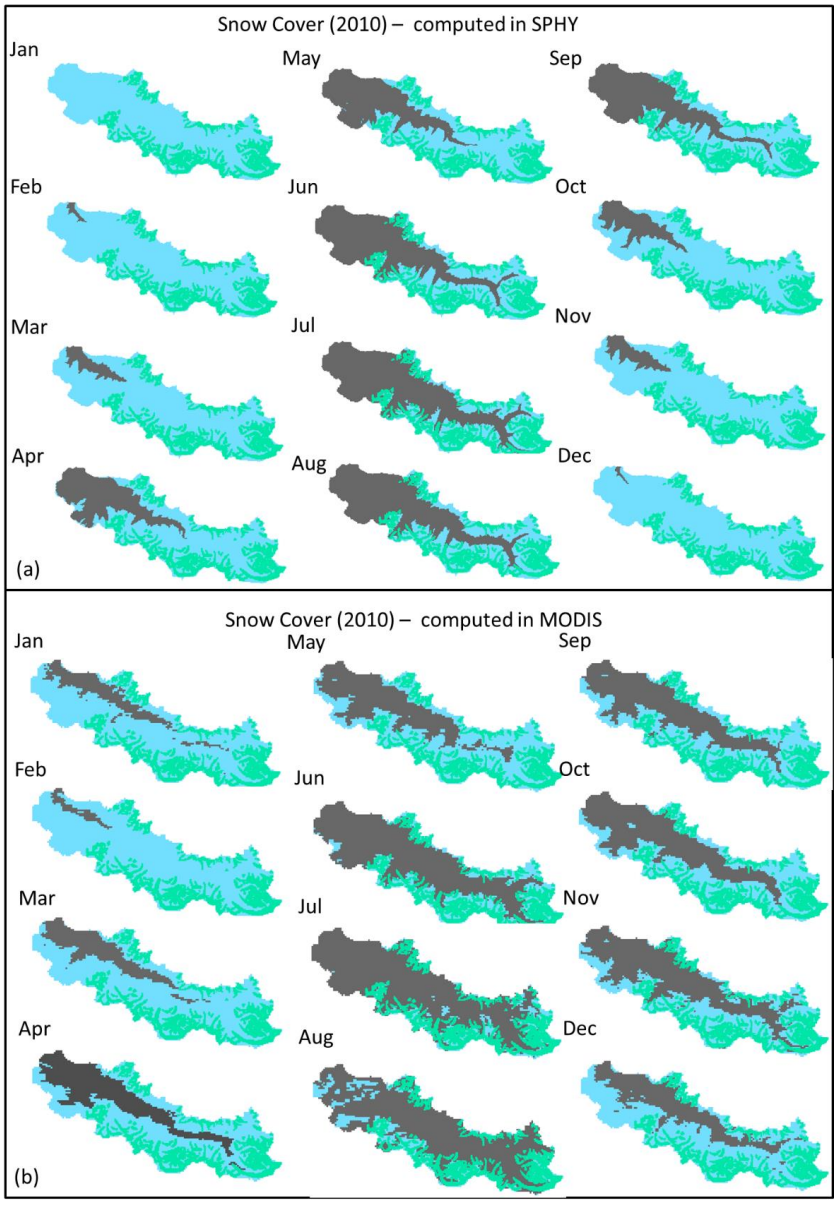

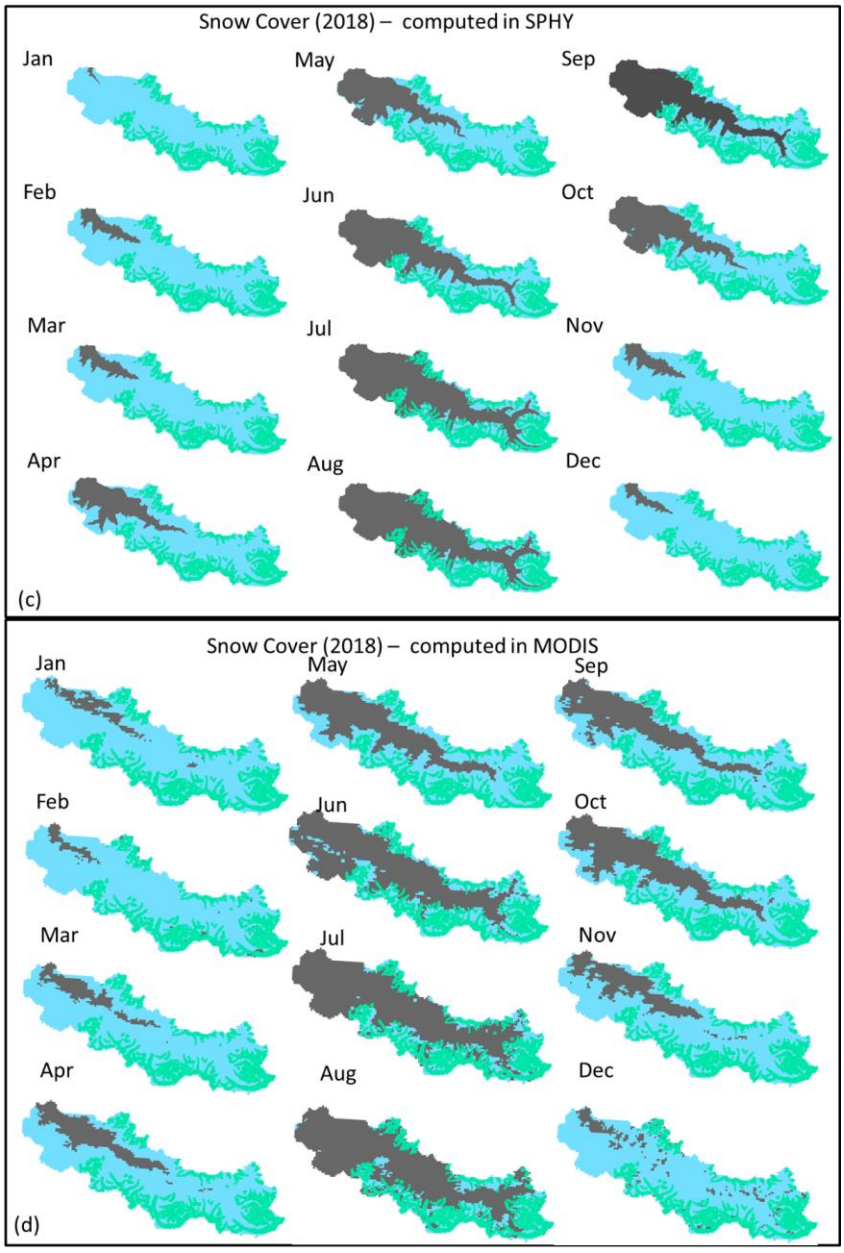

Figure 6: Highlighting similarities and variations in the monthly snow-covered areas (SCA) between MODIS derived snow covers and SPHY derived snow covers: (a) SCAs for 2010 and (b) SCAs for the year 2018.

The regression plots between SPHY and MODIS derived SCAs (%) have been drawn and the corresponding R^2 values have shown in Fig. 7. As per the regression plots (Fig. 7), around 78% correlation existed during 2010 and 92% correlation existed during 2018, which is found quite satisfactory, especially over the Himalayan basin. In Figs. 7a and 7b, except June

to August months, where SPHY derived SCAs show slightly overestimated, otherwise most of months showed a good match between SPHY and MODIS derived SCAs. Several articles already discussed about the inconsistency existed in the MODIS (MOD10A2) snow cover data products (Zhao et al., 2019; Weidinger et al., 2018) due to the presence of clouds. The fractional snow covers based on the 10 elevation zones have been derived for the year 2010 to compare the SPHY derived fractional snow-covered area (%) with the MODIS derived snow-covered areas (Fig. 8).

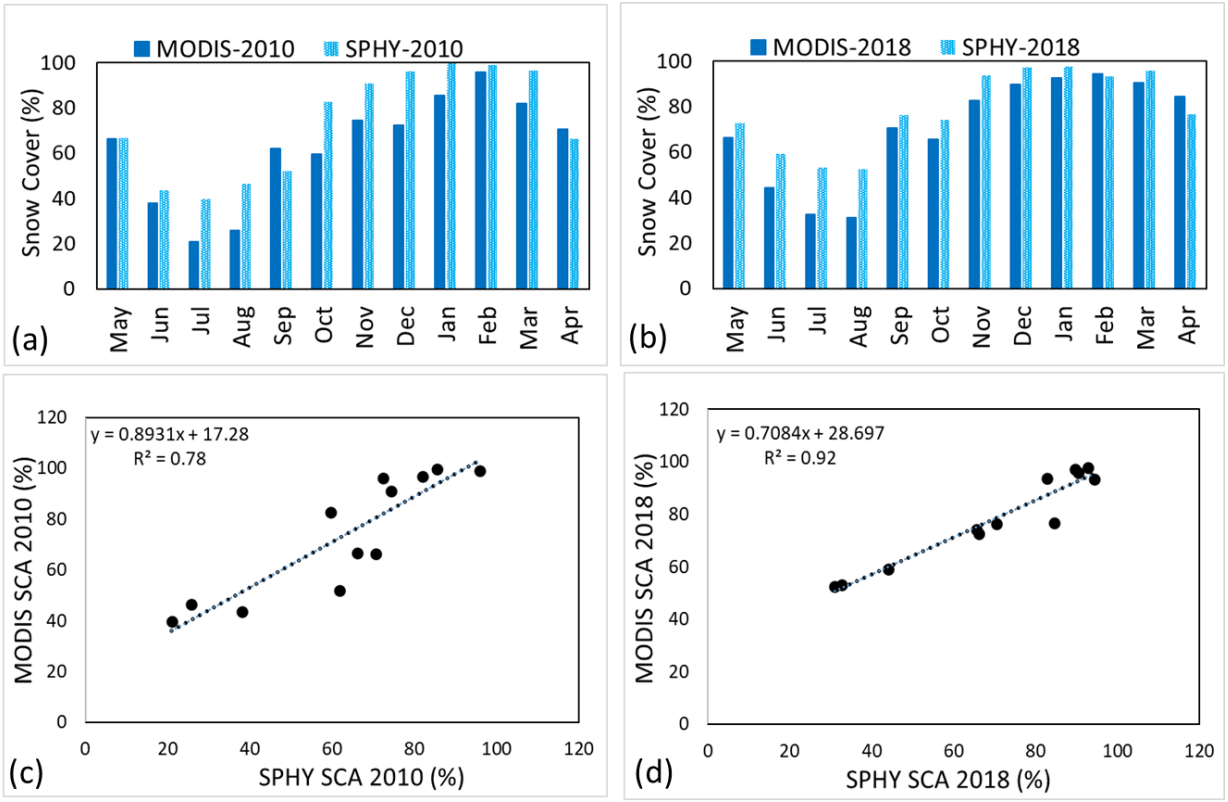

Figures 7: (a) time series plots between MODIS derived monthly SCAs during 2010, (b) time series plots between MODIS derived monthly SCAs during 2018, (c) regression plots showing comparison between observed snow and modelled snow-covered areas (%) during 2010, and (d) regression plots showing comparison between observed snow and modelled snow-covered areas (%) during 2018.

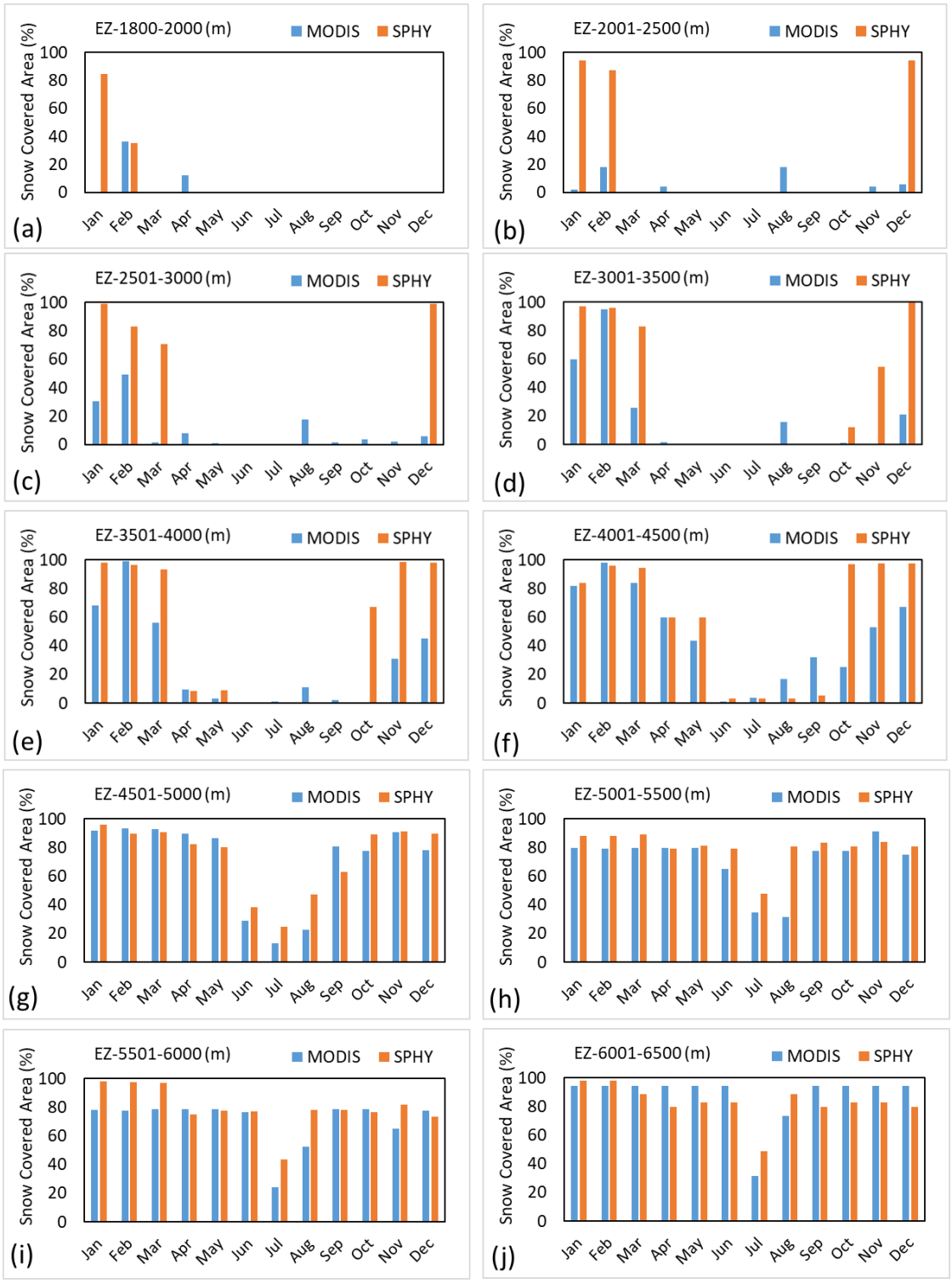

Figure 8: Comparison of SCAs (%) between SPHY and MODIS corresponding to each elevation zone (EZ) during 2010.

Snow cover variations with respect to elevation zones have also been compared. Elevation zones (10 nos.) have computed from DEM (Fig. 1), which highlight the variations in

the snow-covered areas (%) with respect to 10 elevation zones (EZ) through box plots. As per Fig. 1, EZ1 to EZ3 corresponded to lower elevations (1800-3000 m), EZ4 to EZ6 (3001-4500 m) corresponded with moderate elevation areas and EZ7 to EZ10 (>4500 m) corresponded to extreme high elevation areas.

Fig. 8 (a-j) illustrates the monthly comparison of SCA (%) distribution between SPHY and MODIS based on the year 2010. In Fig. 9, it can be observed that as per the increasing EZs, the distribution of SCA increases. In lower EZs such as EZ1 to EZ4, only small amount of SCA can be observed only for January, February and December months, whereas moderate to extreme high EZs > EZ4 most of months show a significant amount of distribution of SCA, except ablation period (i.e. May to August) (Fig. 8). When compared the EZ wise distribution of SCA between MODIS and SPHY, a good correlation has been observed (around 80%), except few EZs where 5% to 10% differences in SCAs (%) has been recorded. Overall, both datasets have shown a good agreement between SPHY and MODIS derived SCAs. Based on the above observations. This elevation zone wise comparison of SPHY derived snow covers with MODIS data showed a good match with the real time MODIS derived snow cover datasets and observed discharge data. The derivation of fractional snow covers also helped to optimize the fractional snow parameter in SPHY, which is an important parameter in accounting snow melt runoff volume.

5.2 Assessment of water balance components

The model parameters have manually adjusted and modeling fitted parameter values detail have been given in the Table 3. The calibration strength of the modeling framework has been tested using coefficient of determination (R^2) (Singh and Goyal, 2017). The scatter plots between observed Q and simulated Q, after parameters adjustment, at Sangla gauge are shown in Figs. 9b and 9d. The time series plots (Fig. 9a and 9c) show that simulated discharge at the

outlet of the catchment significantly captured high and low flow values as per the observed values. The R^2 values are computed as 0.62 and 0.86 for TS1 (i.e. 2003-2010) and TS2 (i.e. 2011-2018), respectively. The computed R^2 values on a daily scale are found satisfactory as compared to the previous studies (Singh and Goyal, 2017; Jain et al., 2010) The modeling accuracy of snow-glacier areas will majorly depend on how snow and glacier parameters are accurately input to the model (Abbaspour et al., 2015).

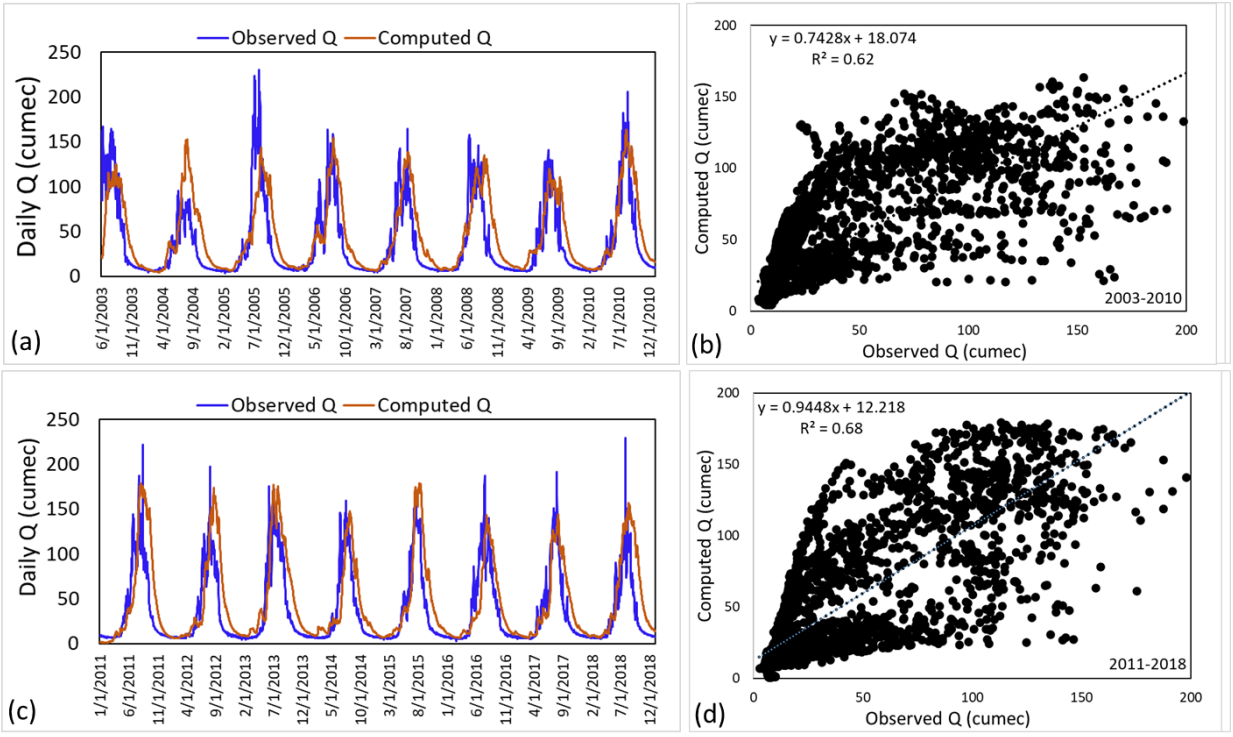

Figure 10: Time series and regression plots showing the comparison between simulated streamflow (including snowmelt and glacier melt) against observed streamflow at Sangla gauge during: (a, b) 2003-2010 and (c, d) 2011-2018.

The water balance components such as simulated runoff (Sim Q, cumec), rain runoff (Rain Q, cumec), snow melt runoff (Snow Q, cumec), glacier melt runoff (Glacier Q, cumec) and baseflow (Base Q) have been computed at the outlet i.e. Sangla gauge (Fig. 10), which shows an average annual distribution of each component during the years 2003 to 2018 in two-time series sets (i.e. TS1: 2003-2010 and TS2: 2011-2018 (total 16 years)). In Figs. (10a-10b),

it is clearly seen that snowmelt contribution (varies from around 50%-52%) is more than glacier melt (varies from around 12%-14%) against the total flow. The contribution of runoff from baseflow is also found significant during May to September months (~15%).

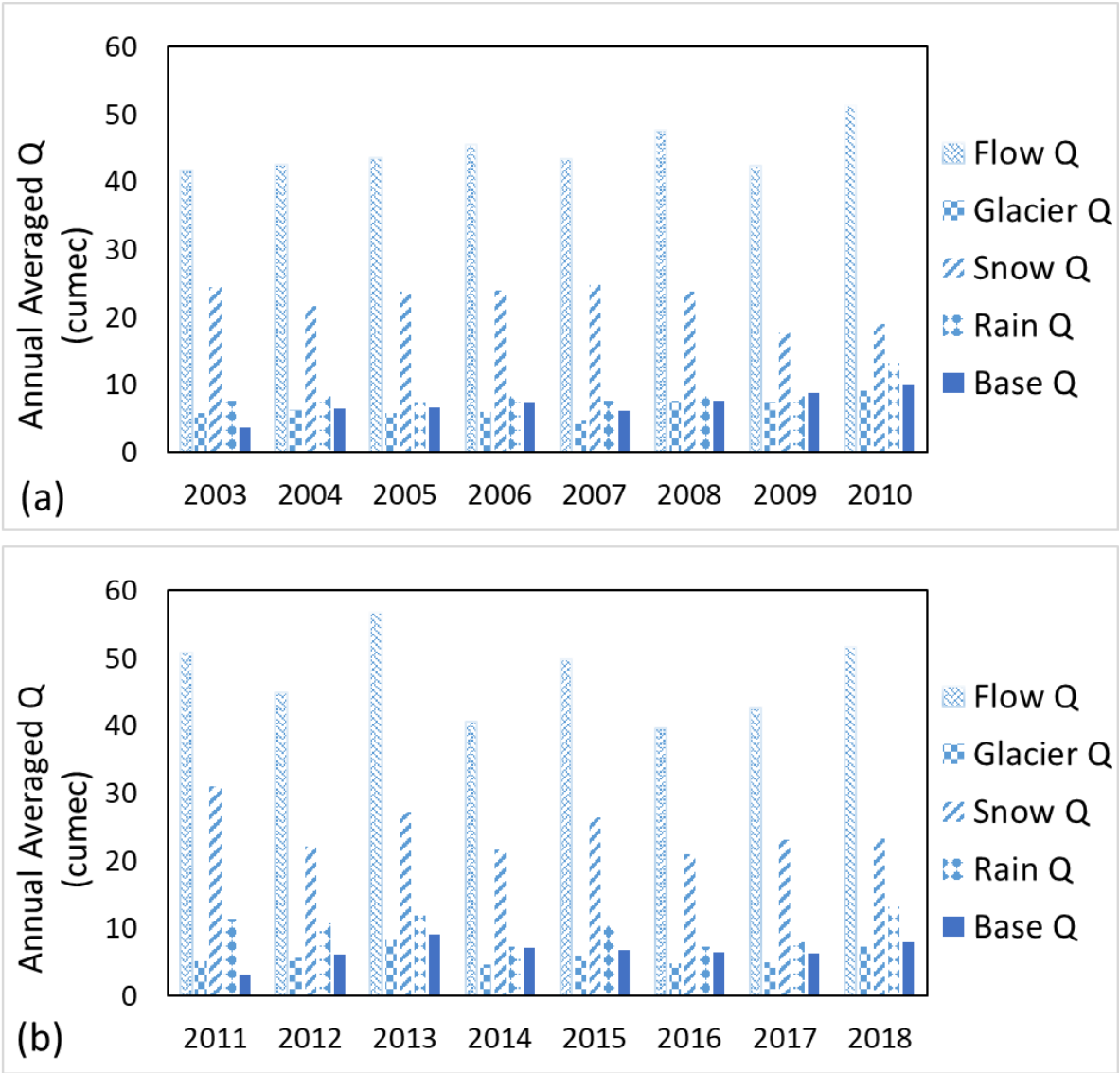

Figure 10: Average annual scenarios of main water balance components such as simulated runoff (Sim Q), Glacier melt runoff (Glacier Q), Snowmelt runoff (Snow Q), rainfall induced runoff (Rain Q) and runoff from the baseflow (Base Q) simulated by SPHY during (a) 2003-2010 and (b) 2011-2018.

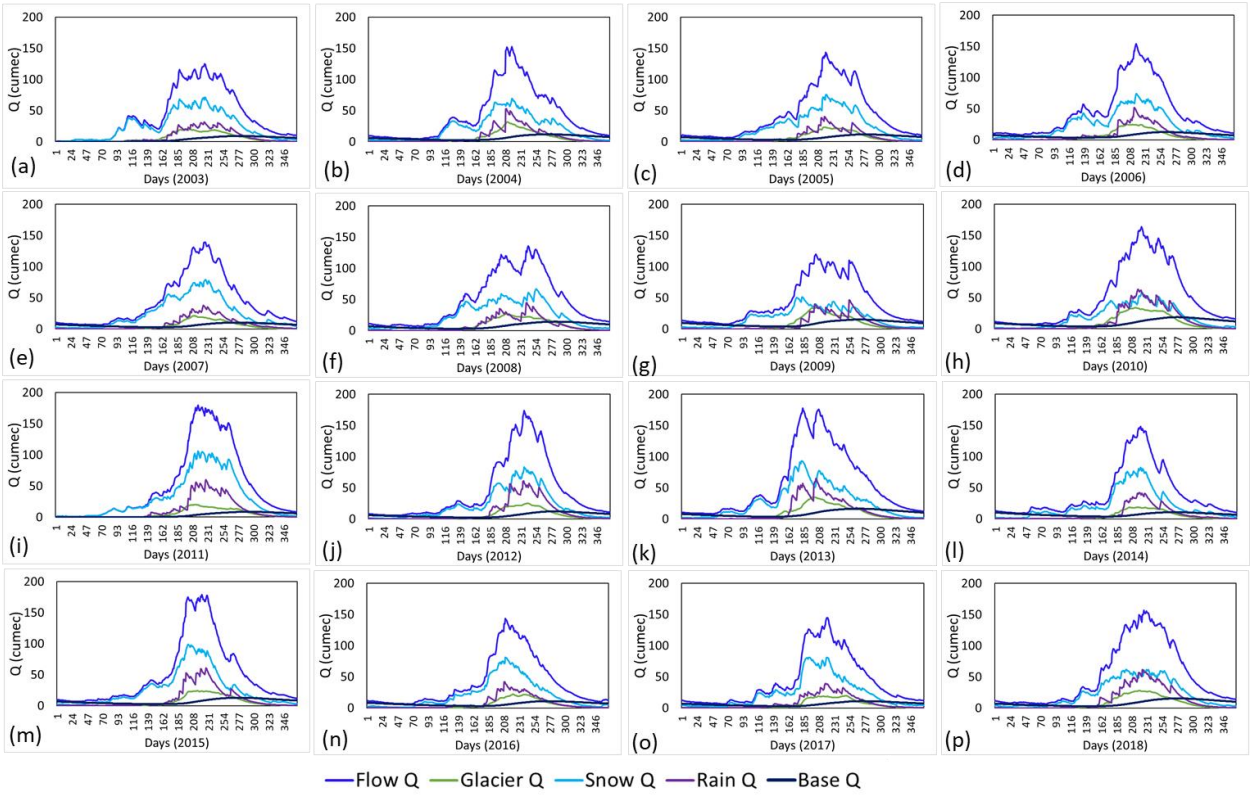

Figure 11: Annual variations in Sim Q, Rain Q, Snow Q, Glacier Q and Base Q computed in during 2003-2018

5.3 Changes in snow melt, glacier melt and rainfall runoff

The contributions of different runoff components (e.g. snow Q, glacier Q, rain Q and base Q) from upstream to downstream have been analyzed. For this purpose, six watersheds viz. Sub 1, Sub 2, Sub 3, Sub 7, Sub 17 and Sub 30 have been selected. In Figure 9, the distribution and amount of runoff components viz. snow Q, glacier Q, rain Q and base Q vary from upstream watersheds to downstream watersheds. Here, the watersheds dominated by snow and glaciers such as Sub1, Sub2 and Sub 3 corresponded to 77% Q from snow-glaciers (i.e. 52% from snow and 25% from glaciers), 62% Q from snow-glaciers (i.e. 21% from snow and 41% from glaciers), and 72% Q from snow-glaciers (i.e. 42% from snow and 30% from glaciers), respectively. Though, the downstream watersheds such as Sub 30 (22% Q from Rain

and 10% from glaciers) and Sub 17 (6% from rain and 16% from glaciers), the melt water contributions from glaciers reduce and the Q from rain is accounted.

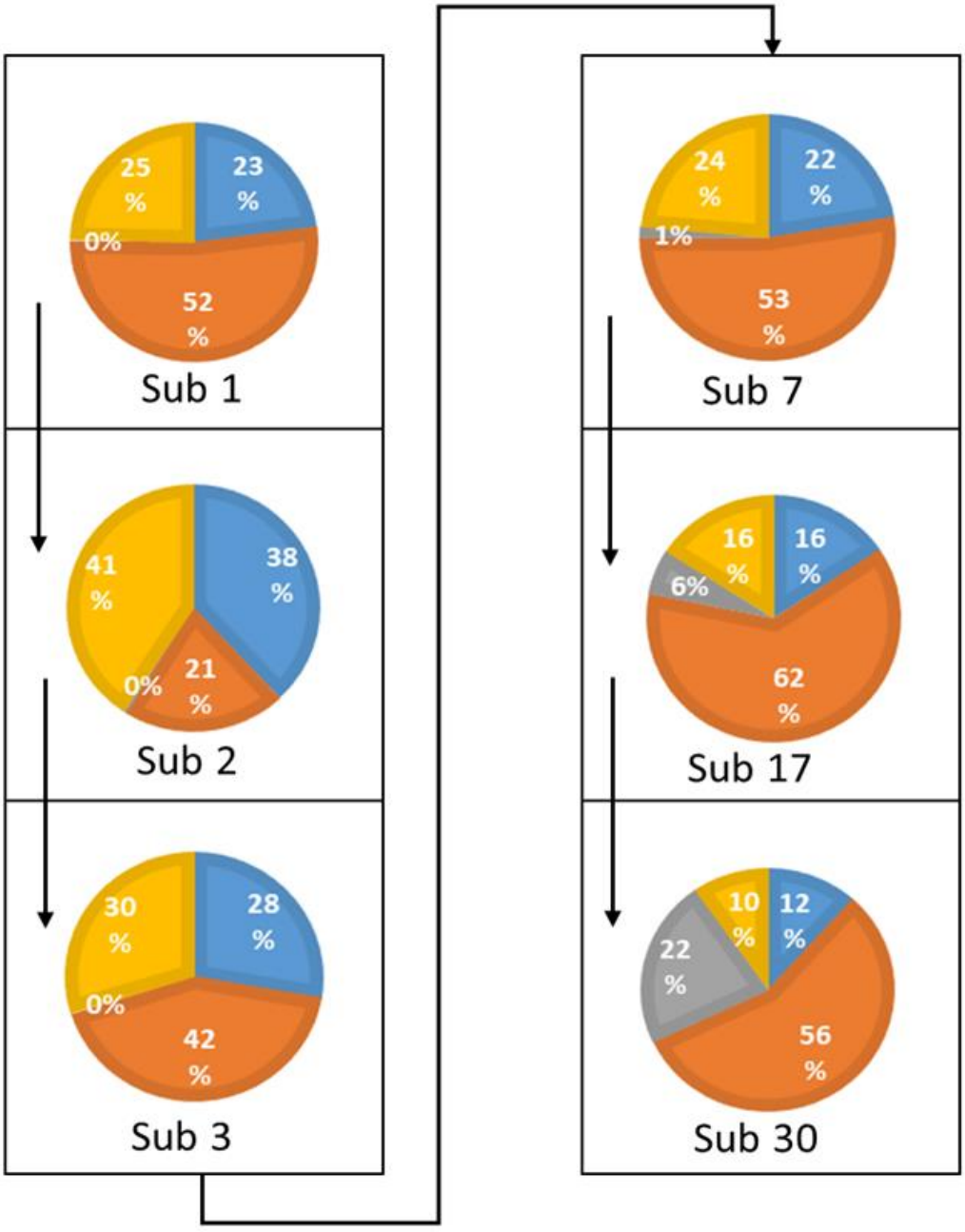

Figure 12: Shows the distribution and amount of runoff components viz. snow Q, glacier Q, rain Q and base Q vary from upstream watersheds to downstream watersheds.

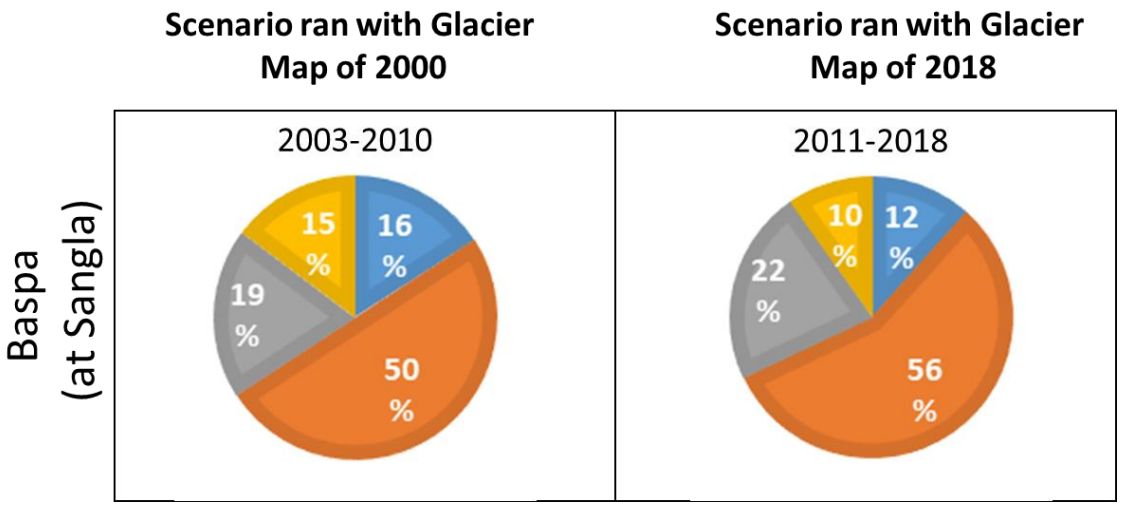

Figure 13: Shows decadal changes in different runoff components at Sangla.

Table 4: Faction (%) of different runoff components at Sangla in Baspa basin.

Runoff Components	**Baspa Basin**
Annual Average **Glacier Melt** Flow at Outlet (m^3/s)	9.78%
Annual Average **Snowmelt** Flow at Outlet (m^3/s)	56.24%
Annual Average **Rainfall Flow** at Outlet (m^3/s)	22.29%
Annual Average **Base Flow** at Outlet (m^3/s)	11.69%

In the above Figure (12) and Table (4), various runoff components contribute to the hydrological regime, reflecting the region's diverse climatic and geographical features. Glacier melt accounts for approximately 9.78% of the total annual flow at the basin outlet, signifying a modest yet critical contribution, particularly during the warmer months. Snowmelt flow, at 56.24%, is the dominant component, highlighting the significant influence of snowpack and seasonal melt in driving runoff, which supports streamflow during the spring and early summer.

Rainfall contributes 22.29% to the annual flow, a substantial portion, especially during the monsoon season, which boosts water availability in the basin. Baseflow, representing groundwater contributions, makes up 11.69% of the total flow, providing a steady release of water that sustains river discharge during dry periods. Together, these components reflect the complex interplay of glacial, snow, and rainfall-driven processes that characterize the hydrology of the Baspa Basin, each playing a vital role in its water dynamics.

Fig. 11 shows distribution of the five main water balance components such as Sim Q (cumec), Snow Q (cumec), Glacier Q (cumec), Rain Q (cumec) and Base Q (cumec) on an annual basis, which highlight the timing of each component throughout the year. As per the annual plots, the potential snow melting starts from April and it continues till October (Fig. 11), however the amount of Snow Q varies from year to year. The maximum Snow Q was computed between late May to July (Fig. 11). The annual total maximum one-day flow recorded around 200 cumec, especially during monsoon season. Whereas, other components such as Snow Q (cumec), Glacier Q (cumec), Rain Q (cumec) and Base Q (cumec) vary one-day maximum up to 120 cumec, 40 cumec, 70 cumec, 20 cumec, respectively. To find out changes in the four main water balance components (e.g. Sim Q, Rain Q, Snow Q, and Glacier Q), the averaged of the water balance components of both TS has been computed and then compared through the box plots (Fig. 14). As per the Sim Q scenarios, a slight increase has been observed from 2003-2010 to 2011-2018, however in case of TS2 (i.e. 2011-2018), the extreme cases were increased and can be seen in box plots (Fig. 14).

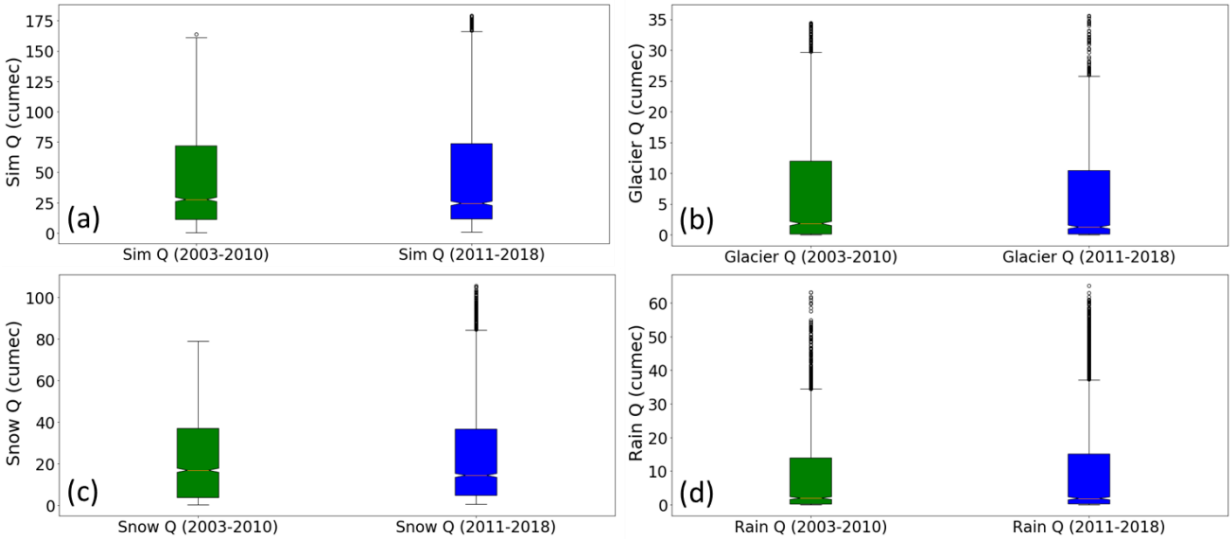

Figure 14: Variations in Sim Q (a), Glacier Q (b), Snow Q (c) and Rain Q (d) computed during two times i.e. 2003-2010 and 2011-2018.

In case of Glacier Q, both time series have shown almost same median (~12 cumec), but in case of TS2 a slight decrease is recorded in upper quantiles (Fig.14). As per Snow Q observation (Fig. 14), TS1 have shown higher values in upper quantile ranges than TS2, but median is recorded almost similar for both TS durations. In case of Rain Q (Fig. 14), except upper quantiles, no significant variability was detected. Based on the above observation, no significant conclusion can be made, however, an enormous variability in upper quantile among all the water balance components can be observed.

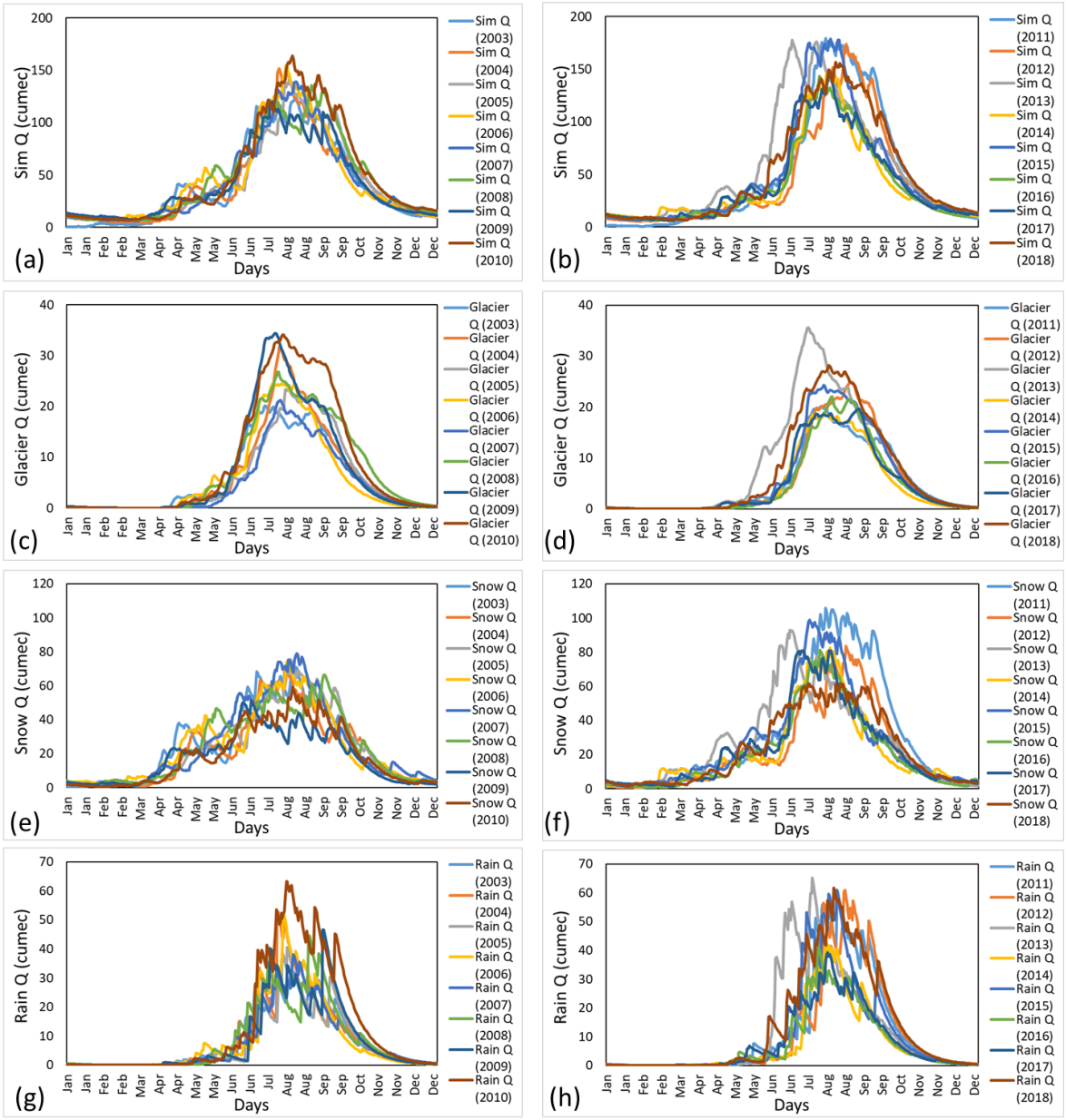

Figure 16: Monthly variations in Sim Q, Snow Q, Glacier Q and Rain Q during the time series sets 2003-2010 (a, c, e, g) and 2011-2018 (b, d, f, h).

Fig. 15 displays the year wise monthly averaged variation in Sim Q, Snow Q, Glacier Q and Rain Q grouped into two TS durations (i.e. 2003-2010 and 2011-2018) computed at the outlet of the basin (i.e. Sangla gauge). These plots highlight a year-to-year variability in monthly averaged components. In case of Sim Q (Figs. 15a to 15b), the highest variability has been recorded from June to September months (mainly in the monsoon months). The variability

in the Q during monsoon (i.e. from June to September) months revealed the existed variability in precipitation and temperature observed in recent past year (Rao et al., 2018; Singh and Goyal, 2017). Similar observations can be notified for Snow Q during Mar to May. For example, as per Figs. (15e to 15f), during 2011-2014 the maximum Snow Q (120 cumec) was recorded for the year 2014, while other years recorded maximum Snow Q between 60 cumec to 100 cumec. In case of Glacier Q (Figs. 15c and 15d), no significant variability has been recorded, however, the month wise change can be observed in the glacier amount. In case of Rain Q (Fig. 15g to 15h), the maximum variability (e.g. extreme high and low peaks) during monsoon months can be clearly observed.

As discussed above, it was observed that there are changes in water balance components because of changes in precipitation and temperatures. As per the studies carried out earlier in Himalaya region average temperature has been increased over the Himalaya (~1°C) (Dimri et al., 2018; Sanjay et al., 2017) and the precipitation significantly varied over western Himalaya, especially in recent past years (Sharma and Goyal, 2020; Shafiq et al., 2016; Singh and Goyal, 2016). Therefore, a detail analysis of change has been performed by doing the monthly assessment of the main four water balance components (i.e. Sim Q, Snow Q, Rain Q and Glacier Q). To find out the changes during both the TS durations (i.e. 2003-2010 and 2011-2018) among all four water balance components, the monthly scenarios (Figs. 16a and 16b) have been generated and a comparative assessment has been done between TS1 (i.e. 2003-2010) and TS2 (2011-2018). As per Sim Q (Fig. 16a), it is found highly variable throughout the year. As per December to March, July and July trends (Fig. 16a), Sim Q is increased during both TS. During April, May, August, September and October (Fig. 16b), Sim Q is slightly decreased. In October and September, Sim Q scenarios from 2003-2010 showed an increase, while 2011-2018

Table 5: Shows the changes in different runoff components at each watershed under different scenarios.

Stations	2003-2010 - run with Glacier map of 2000					2011-2018 run with Glacier map of 2018				
	Sim flow	**Glacier melt**	**Snow melt**	**Rain flow**	**Base flow**	**Sim flow**	**Glacier melt**	**Snow melt**	**Rain flow**	**Base flow**
1	1002.0	297.0	427.1	4.0	273.9	1097.3	269.6	573.1	3.0	251.6
2	1286.3	506.5	303.7	6.5	469.6	1517.9	618.5	315.7	5.9	577.8
3	579.0	190.2	213.1	2.0	173.6	696.5	207.3	294.9	1.1	193.2
5	902.3	267.3	383.0	6.0	246.0	976.0	222.3	540.7	5.4	207.5
8	666.1	142.8	390.3	1.9	131.1	644.9	31.1	582.0	2.7	29.1
9	775.7	114.8	546.0	9.9	105.0	759.4	34.6	684.5	8.0	32.3
11	543.5	151.3	249.8	4.0	138.4	545.2	84.0	379.6	3.5	78.0
12	845.3	224.0	407.4	6.5	207.4	794.1	55.1	682.5	5.3	51.1
14	366.6	172.2	38.5	0.2	155.7	377.0	167.3	54.3	0.1	155.2
16	872.8	243.1	373.5	28.6	227.6	955.9	244.4	439.4	38.8	233.3
18	1272.6	435.7	429.1	4.0	403.8	1327.3	316.1	712.8	3.1	295.3
20	1643.4	324.2	814.9	197.7	306.6	1594.4	144.1	1067.6	242.0	140.6
21	2212.3	605.5	972.7	59.5	574.5	1880.1	283.1	1222.6	91.1	283.3
23	2127.4	703.4	748.3	18.8	657.0	1718.1	155.8	1383.2	33.4	145.7
24	2664.8	932.0	820.9	38.7	873.2	1826.2	185.2	1389.1	78.6	173.2
25	2290.2	591.0	912.8	222.3	564.0	1751.6	92.6	1255.7	304.8	98.5
26	3048.4	1199.7	675.7	42.7	1130.3	2557.1	820.7	844.4	91.8	800.3

In case of TS2, January to March, an increase has been observed. Similarly, during October to March as per TS1, Rain Q has been decreased, while in TS2, February and March showed an increase in Rain Q. But as per TS2, during January, February, March, August and September, it has been increased (Fig. 16a). Overall, majority of plots showed that Rain Q has been slightly increase during 2003 to 2018. As per Glacier Q plots (Fig16b), during October to

December, a slight decrease in Glacier Q has been reported during 2011-2018, while an increase is reported as per 2003-2010. However, from January to September, most of the plots showed an increase in Glacier Q in both TS, except April (in case of both TS) (Fig. 16b) and September (in case of TS2 only), where Glacier Q was slightly decreased (Fig. 16). Snow Q is found highly variable in both TS (i.e. 2003-2010 and 2011-2018) from October to September. Snow Q trends showed that it is decreased during October, November, March and April (in case of both TS durations). Whereas, it is significantly increased in December, January, February, May, June and July, mostly in case of TS2 (i.e. 2011-2018) (Figs. 16b). During April to September (Fig. 16d), it is decreased in most of months, especially in case of TS1 (i.e. 2003-2011). Overall, plots clarified that with respect to TS1 (i.e. 2003-2010), the contribution of Snow Q in total runoff has been increased during 2011 to 2018.

Based on the above observation, the three most conclusive observations can be made: (i) Rain Q is found highly variable during 2003-2018, because the most of months during 2003-2010 have shown a decrease in Rain Q and during TS2 (i.e. 2011-2018) with respect to TS1, it is increased during January, February, March, August and September months, (ii) overall the Snow Q was increased while comparing TS1 vs TS2 (Table 5). However, because of an increasing temperature over the Himalaya, as reported in previous studies (Shafiq et al., 2016; Singh and Goyal, 2016), the ratio of precipitation to snow and rain is changing. Therefore, due to less amount of precipitation (in form of snowfall), the melt contribution from Snow has been decreased in some months (mostly in non-glaciated areas) and therefore Rain Q was increased during January, February and March. Due to the increasing temperature and reduction in the glacier mass over Himalaya, the contribution from Glacier Q was decreased during TS2 as compared to the TS1 (Table 5). Table 5 showed the observations from 17 stations, which are found glacier dominated.

Figure 16: Month wise variations and trends in Sim Q, Rain Q, Glacier Q and Snow Q: (a) variations in Sim Q and Rain Q, (b) variations in Glacier Q and Snow Q.

5.4 Effect of glacier area reduction in glacier melt runoff

For effective monitoring the changes in snow and glacier melt runoff, around 30 watersheds were drawn in the basin taking, out of these 17 sites dominated with glaciers and snow-covered areas as shown in Fig. 1 and then the annual time series trends were estimated during 2003-2018 (Fig. 11). In this analysis, one more glacier map of 2018 was used in addition to 2011 for the duration TS2.

The glacier melt runoff contribution at the outlet during 2003-2010 computed as ~15 % (as per glacier map of 2000), it computed ~13% during 2011-2018 (as per glacier map of 2011) and it recorded around ~10% during 2011-2018 (as per glacier map of 2018), due to reduction in glacier mass. Similarly, the snow melt runoff contribution was found to be 50,52 and 56% and rainfall runoff 19, 21 and 22% and base flow contribution 16,14 and 12% corresponding to the maps of 2000, 2011 and 2018. This base flow is delayed runoff which comes through recharge from rain, snow and glacier melt. If it is distributed in same proportion then runoff comes out to be 18,15,12% due to glacier melt, 58,61,64% due to snowmelt for the years 2000, 2011 and 2018 and rainfall runoff 24% for all the years.

All the watersheds are having different snow/glacier therefore the total contribution of melt water from snow covered areas and glacier areas varies at each site level. The contribution from each watershed is shown in Fig. 17 and given in Table 5. The glacier melt runoff varies from around 200 mm (corresponded to Site 9) to 1500 mm (corresponded to Site 26) across all stations. Similar plots have been made for snow melt runoff (i.e. Snow Q), which varies from around 40 mm (corresponded to Sites 8 and 9) to 350 mm (corresponded to Site 26). In Fig. 17, among 17 sites (mostly dominated with glaciers), most of sites showed an increase in Snow Q during 2003 to 2018.

From Table 3, it can be seen that glacier melt runoff has increased in case of watersheds 2 and 3 while decreased for other watersheds. The reason behind this that the watersheds 2 and 3 are heavily glaciated and also not much change in glacier cover have been found in these watersheds. The watershed such as 8, 9 and 12 located on northern side in high altitude areas have lost much glaciers as compared to watersheds located on Southern side. Therefore, more reduction in runoff in watersheds of northern side was observed. The watersheds 21,23,24,25 and 26 located on lower altitudes have lost much glacier area and therefore contribution in these watersheds have been found to be much less in the year 2018. However, contribution of

change of SCA and rainfall also have been studied. The snow melt runoff from all the watersheds have increased.

Figure 17: Annual variations and trends in Snow Q and Glacier Q across 17 stations out of 30 stations dominated with snow and glaciers during 2003-2018.

Fig. 18 shows the month wise comparison of glacier melt runoff (Glacier Q) changes and snow melt runoff (Snow Q) between TS1 (i.e. 2003-2010) and TS2 (i.e. 2011-2018) for 17 sites dominated by snow-covered areas and glaciers. The computation of monthly distribution

of amount of Snow Q and Glacier Q at Site level has been found helpful to understand the behavior of total Q, while analysing the variability of Glacier Q and Snow Q in total runoff. In Baspa basin, the Glacier melting mostly starts from May and the majority of contribution from Glacier Q is recorded till November (>10 mm). Similarly, in case of Snow Q, the major contribution is recorded from late April to October (>10 mm). Therefore, the box plots have shown the monthly scenarios of Glacier Q and Snow Q from May to October months only. The Box plots highlighted the statistical behaviour of different grouped periods. As per Figs. 18, in case of Glacier Q, it can be seen that maximum amount is recorded during July to September. When compared to TS1 vs TS2, a shift in Glacier Q can be observed. In most of the stations a slight reduction in the amount of Glacier Q was observed during 2011-2018 against 2003-2010. As per the glacier maps of different time periods, it can be seen that the small size glaciers were found more sensitive in reducing their mass. This explores the monthly fluctuations on the yearly basis in Snow Q and Glacier Q and also provides the ideas about the Snow Q dominant season and Glacier Q dominant season throughout the year.

Fig. 18 also displays the changes in monthly Snow Q during 2003-2018 for 17 sites dominated with snow and glaciers. As per the comparison of grouped time series sets (i.e. TS1 and TS2), most of months found highly variable in case of Snow Q. Overall, most months showed increase in Snow Q during 2011-2018 with respect to TS2 (i.e. 2003-2010) (Fig. 18 and Table 5). The increase in Snow Q over glaciated areas can be directly correlated with the reduction of Snowfall over the basin due to increasing rate of temperature over Himalayan glaciers. As temperature increases, snowfall contribution decreases and rainfall contribution increases.

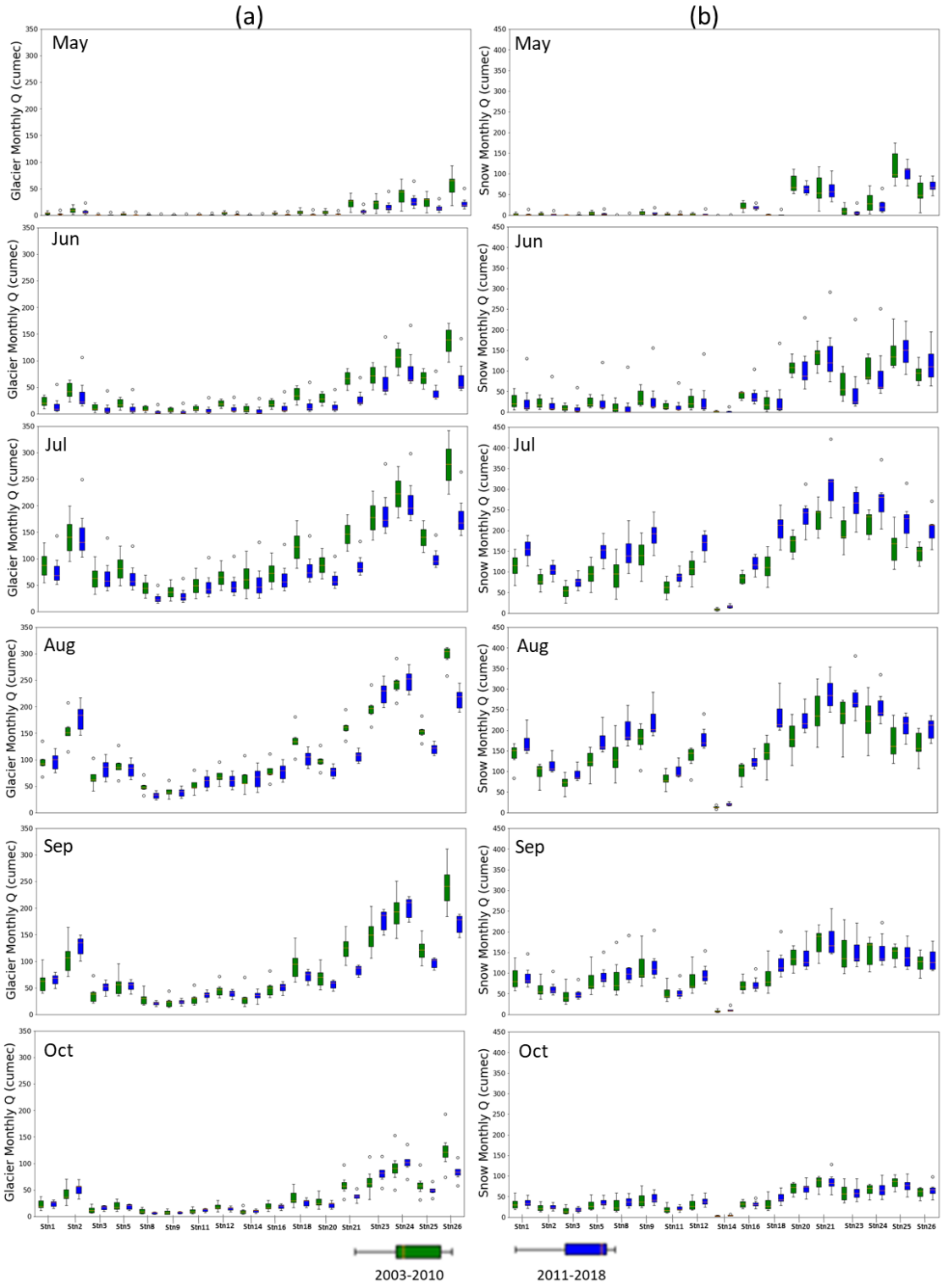

Figure 18: Monthly variations in (a) Glacier Q and (b) Snow Q across 17 stations dominated with snow and glaciers during 2003-2018.

In Fig. 19 (a to d), a significant amount of glacier area reduction has been computed. Fig. 19 shows the hypsometry of glaciers in different temporal times. Here, hypsometry of glaciers has been calculated to determine the cumulative percentage of glacier area between the elevation zones. Total six elevation zones, at 500-m interval, have been calculated. The hypsometry of all glacier maps clearly shows that a significant reduction in the lower to extreme elevation areas. When compared to glacier map of 2000 with 2006, a very slight reduction in the glacier areas can only be observed, especially between 6000-6500 m ranges. However, there is a large gap can be observed at lower to moderate elevation zones (e.g. 4500-5000 m) in the glacier maps of 2011 and 2018 vis a vis glacier map of 2000. These changes could be a sign of elevation dependent warming, as also discussed previously in some Himalayan based studies (Dimri et al., 2018; Singh and Goyal, 2016). This analysis gives an insight about the sensitivity of glacier areas changes with respect to elevation.

Table 6: Changes in glacier areas in different times in the Baspa River basin.

SI No.	Year	Aggregate area km^2	Glacier Loss from 2000 (in Km^2 Area)	Average Glacier Loss from 2000 (in Km^2 Area)	Glacier Volume, km^3 (as per Prasad et al., 2019)	Glacier Volume, km^3 (as per SPHY modeled)
1	2000	212.93	NA	–	13.09	13.41
2	2006	203.86	9.07	9.07	12.46	12.84
3	2011	184.12	28.81	19.94	11.12	11.6
4	2018	174.41	**38.52**	**25.46**	10.47	10.99

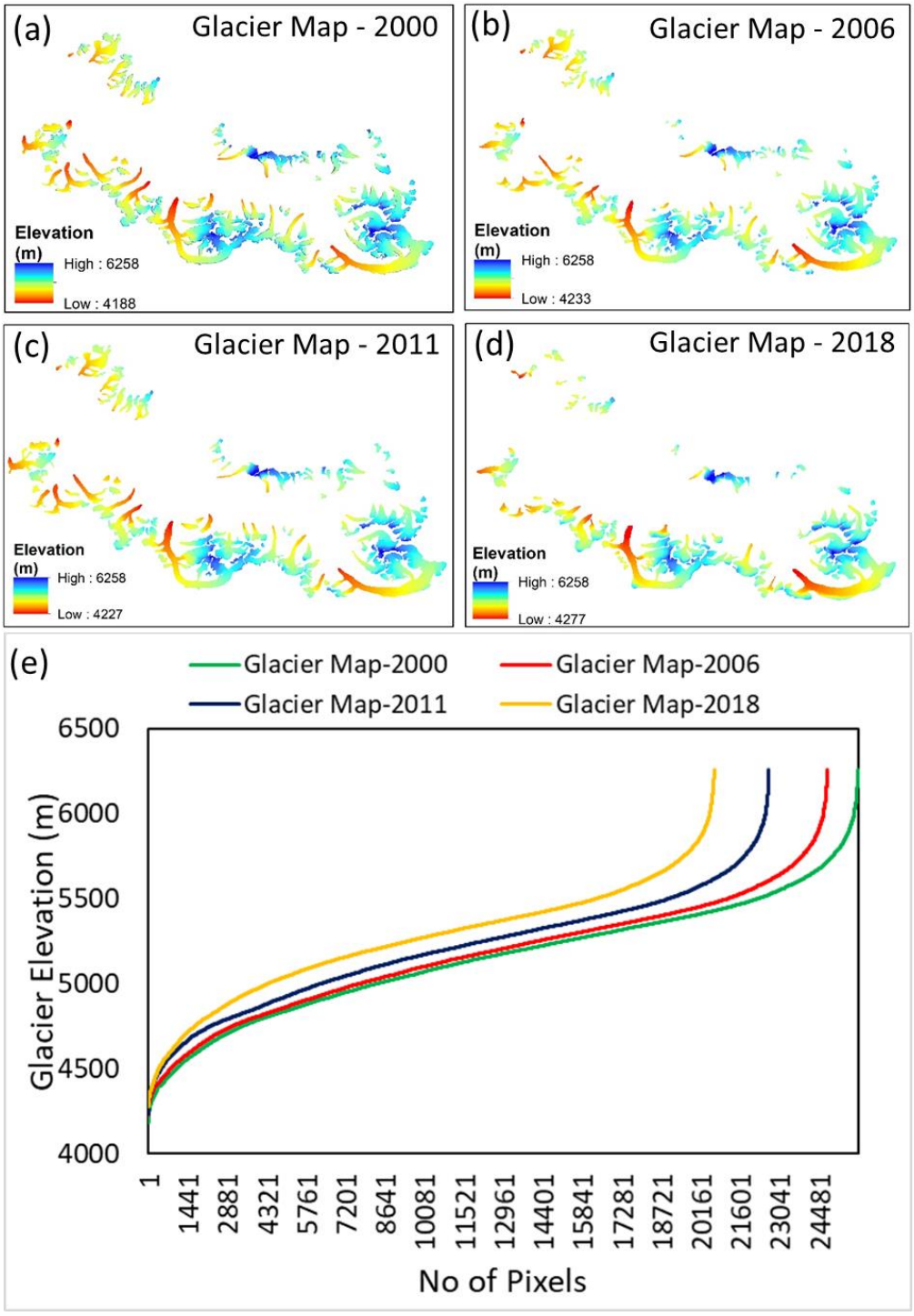

Figure 19: Highlighting changes in glacier maps during (a) 2000, (b) 2006, (c) 2011, (d) 2018 and (e) comparing variations in glacier maps corresponded to elevations.

The glacier ice volume has been computed to verify the reduction in the glaciers ice volume as per the changes in glacier maps with respect to time. To compare the reduction in glacier ice volume due to melting, SPHY based glacier ice volume compared with the glacier ice volume computed based on the power equation suggested by Prasad et al. (2019). Prasad et al. (2019) developed a volume-area relationship considering 298 glaciers, which are mostly corresponded to Satluj river basin. The glacier ice volume has been computed for the four different temporal glacier maps (i.e. 2000, 2006, 2011 and 2018) using above two methods and given in Table 6. In 2000 the total glacier ice volume was recorded around 13.09-13.41 Km^3, while in 2018, it was significantly reduced (recorded as 13.47-10.99 Km^3). As per the comparison, SPHY has found comparable in the calculation of glacier ice volume with respect to the glacier ice volume computed through the volume-area equation.

Table 7: Shows the changes in different sizes of glaciers in the randomly selected watersheds.

Basins	**Size**	**Small Size Glaciers (<=30 km^2)**			**Large Size Glaciers (>30 km^2)**
BRB	Years/Sub Nos	Sub 1	Sub 5	Sub 2	Sub 3
	2000	4.56	7.54	12.19	33.89
	2018	4.43	6.38	12.02	33.62

Table 7 shows the area change in the selected watersheds. In Table 7, it is observed that the small size glaciers have significantly reduced their size in the different decadal times as compared to large size glaciers in the Baspa basin. Figures 19 and 20 show the change in glacier areas for the selected watersheds in and daily mean glacier Q (m^3/s) with respect to each watershed. Here, the Sub 5 and Sub 1 show noticeable reduction in the glacier Q and the same change can be visualized in Figure 20, which shows significant reductions in the glacier Q (e.g. for Sub 5, it varies from 30% to 23% and for Sub 1, it varies from 30% to 25%) and base Q (i.e. from 27% to 21% and 27% to 23%), while the snow Q shows enhancement (i.e. 42% to

55% and 43% to 52%). In case of Sub 3 and Sub 2, the glacier Q has shown increase from HS1 to HS2 (i.e. increases from 192.2 to 207.3 in case of Sub 3 and in case of Sub 2, it increases from 506.7 to 618.7).

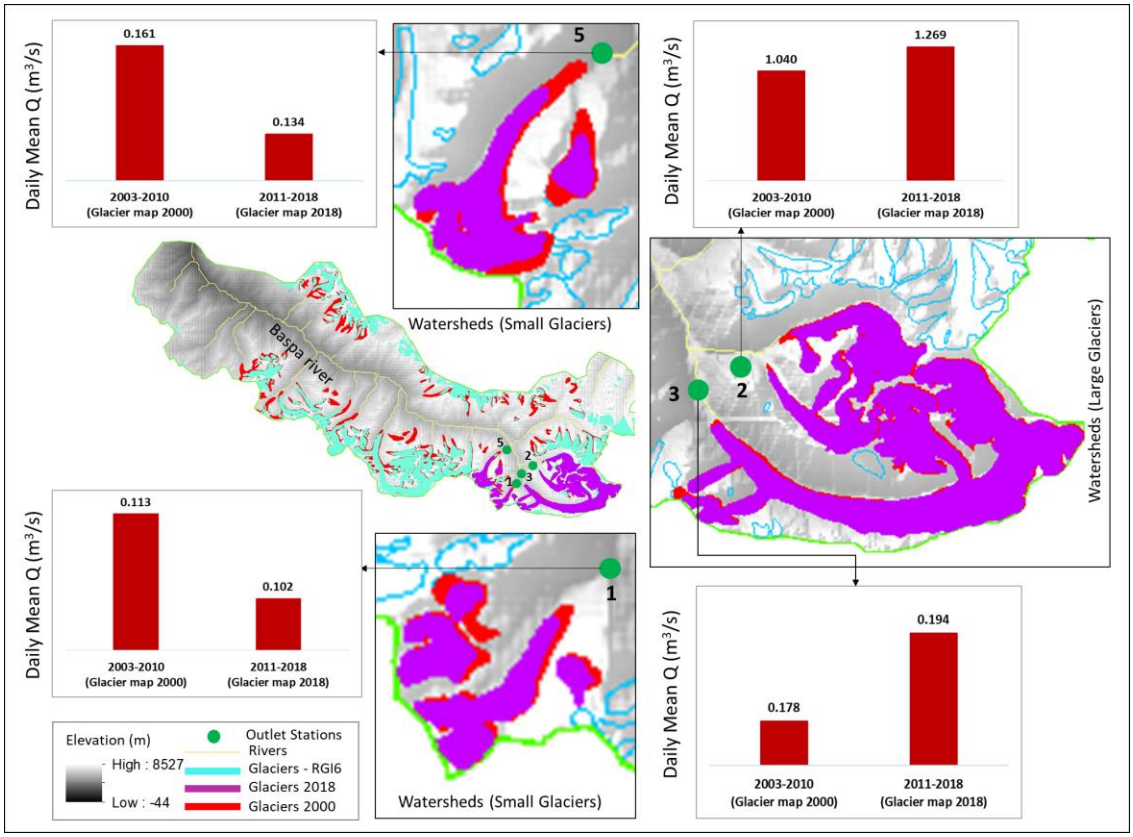

Figure 20: Glacier area and glacier melt runoff (glacier Q, daily mean in m^3/s) changes as per selected watersheds comprises with large size and small size glaciers in BRB.

5.5 Long-term Changes in Snow Cover in Baspa Basin

The Figure 21 illustrates the long-term variation in snow cover percentage from 1951 to 2014 in a historical context. The snow cover exhibits a clear cyclical pattern, with regular peaks and troughs reflecting seasonal variations in snow accumulation and melt. The overall trend shows a general decline in snow cover percentage over the studied period. This gradual decrease is highlighted by the red line, indicating a downward trend, which could be attributed to the long-term effects of climate change, such as rising temperatures and altered precipitation

patterns. The amplitude of the cycles remains relatively consistent, implying that while seasonal variability persists, the baseline snow cover is steadily decreasing. This decline suggests potential impacts on water resources, particularly in regions dependent on snowmelt for river flow, such as high-altitude basins. The reduction in snow cover could also affect the timing and volume of runoff, potentially exacerbating issues like water scarcity or changing flood regimes. Overall, this data underscores the importance of monitoring snow cover trends, as they are critical indicators of broader climatic changes and have significant hydrological and environmental implications (Fig. 21).

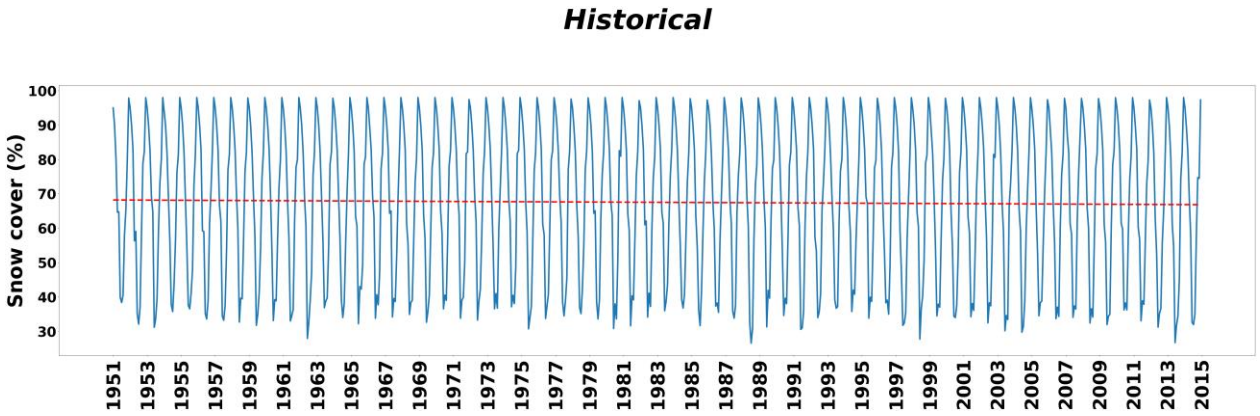

Figure 21: Shows the long-term change in snow cover (%) in the Historical time during 1951-2014.

The projected change in snow cover percentage from 2015 to 2100 under the CMIP6 SSP245 scenario shows a significant and consistent decline. SSP245 represents a "middle-of-the-road" scenario, where some mitigation efforts are made but emissions and temperature rise continue at moderate levels (Fig. 22). As per the projections, snow cover percentages steadily decrease over the century, reflecting the increasing influence of temperature changes (increase) in the Baspa basin. The reduction in snow cover is particularly noticeable after mid-century, with the rate of decline accelerating. This is likely due to rising temperatures, which reduce the duration and extent of snow accumulation, especially at lower elevations and in mid-latitude

regions of the Baspa basin. The projected loss of snow cover can have profound impacts on river flows in the Baspa basin, particularly in snow-fed regions, as snowmelt plays a crucial role in sustaining streamflow during dry months.

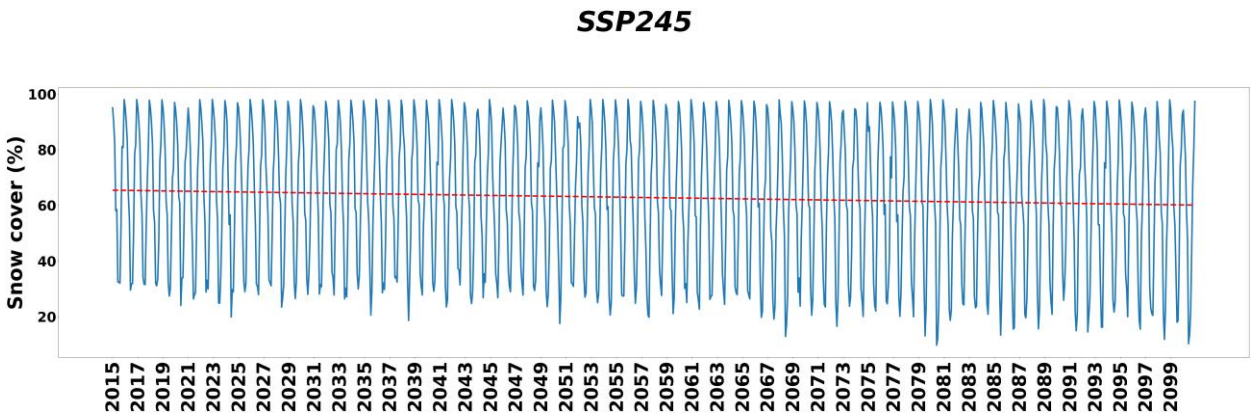

Figure 22: Shows the long-term change in snow cover (%) during 2015-2100 as per (CMIP6 Models) SSP245.

The Fig. 23 showing the long-term change in snow cover percentage from 2015 to 2100 under the CMIP6 SSP585 scenario presents a significant downward trend. SSP585 represents a high-emission scenario where limited efforts are made to mitigate greenhouse gas emissions, leading to substantial global warming. The snow cover percentage steadily decreases throughout the century, with sharper declines observed in the later decades, reflecting the impacts of increasingly warmer temperatures. This accelerated reduction in snow cover under SSP585 highlights the drastic effects of unchecked climate change on seasonal snow dynamics. By the end of the century, snow cover is projected to be significantly lower compared to earlier periods.

When comparing the SSP585, SSP245, and historical trends, notable differences emerge. The historical graph (1951-2014) shows relatively stable snow cover with some decline, but seasonal variability persists. Under SSP245 (2015-2100), the snow cover decreases more noticeably but at a moderate pace, indicating that some mitigation efforts slow the rate

of decline. The SSP245 scenario reflects a scenario where mitigation policies slightly curb emissions, resulting in a slower but still evident reduction in snow cover. In contrast, SSP585 shows the most dramatic reduction in snow cover, especially after 2050, as global temperatures rise rapidly. This noticeable difference between SSP245 and SSP585 underscores the critical importance of mitigation measures. While both scenarios project declines, the rate and severity are far worse in SSP585. The decreasing snow cover in both future scenarios compared to historical data also emphasizes the long-term impacts of climate change. The loss of snow cover in the future will have cascading effects on the streamflow in the downstream parts of the basin.

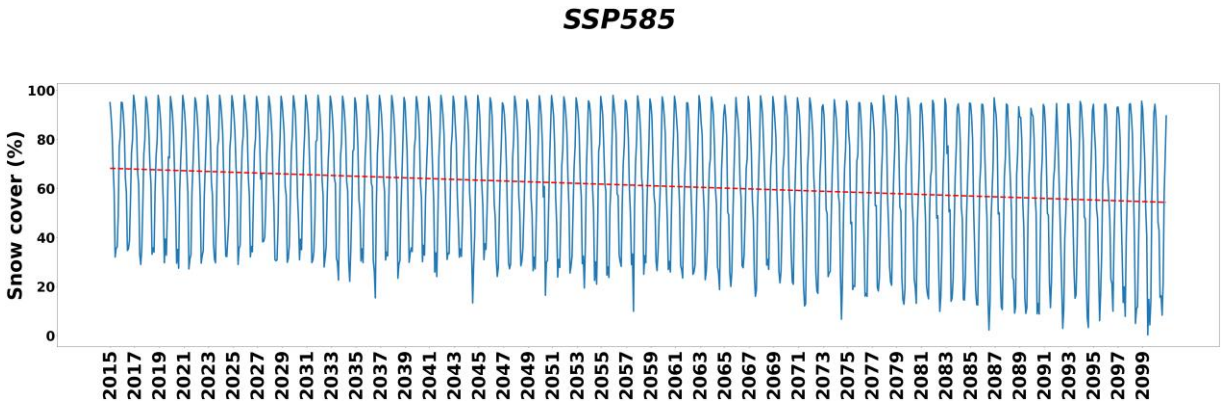

Figure 23: Figure 2: Shows the long-term change in snow cover (%) during 2015-2100 as per (CMIP6 Models) SSP245.

5.6 Climate Change Impact Assessment on Different Runoff Components

The Fig. 24 provides a comparative analysis of runoff components i.e. Total Q, Rain Q, Snow Q, and Glacier Q under SSP245 and SSP585 scenarios over time (2015-2100) in reference to base line time (i.e. 1980-2014). Here it can be seen that total runoff (Total Q) increases significantly over time, with SSP585 (orange line) showing much higher peaks, particularly after 2050, compared to SSP245 (blue line). This reflects the stronger impact of

higher emissions in SSP585 on total runoff, likely driven by increased rainfall and glacial melt. The top-right panel illustrates that rainfall runoff (Rain Q) also increases sharply, particularly in SSP585, where the peaks become more frequent and intense towards the end of the century, indicating higher rainfall events under a warmer climate. The Fig. 25 also reveals that glacial runoff (Glacier Q) increases steadily in both scenarios, but SSP585 shows a more dramatic rise after 2060, reflecting accelerated glacier melt due to higher temperatures. The bottom-right panel highlights the decrease in snowmelt runoff (Snow Q), with both scenarios showing a downward trend, but SSP585 experiences a more pronounced decline. This indicates a shift from snow-driven runoff to rain and glacier-driven runoff in the future, with more extreme variations under SSP585. Collectively, the figure underscores the substantial hydrological shifts expected under different climate scenarios.

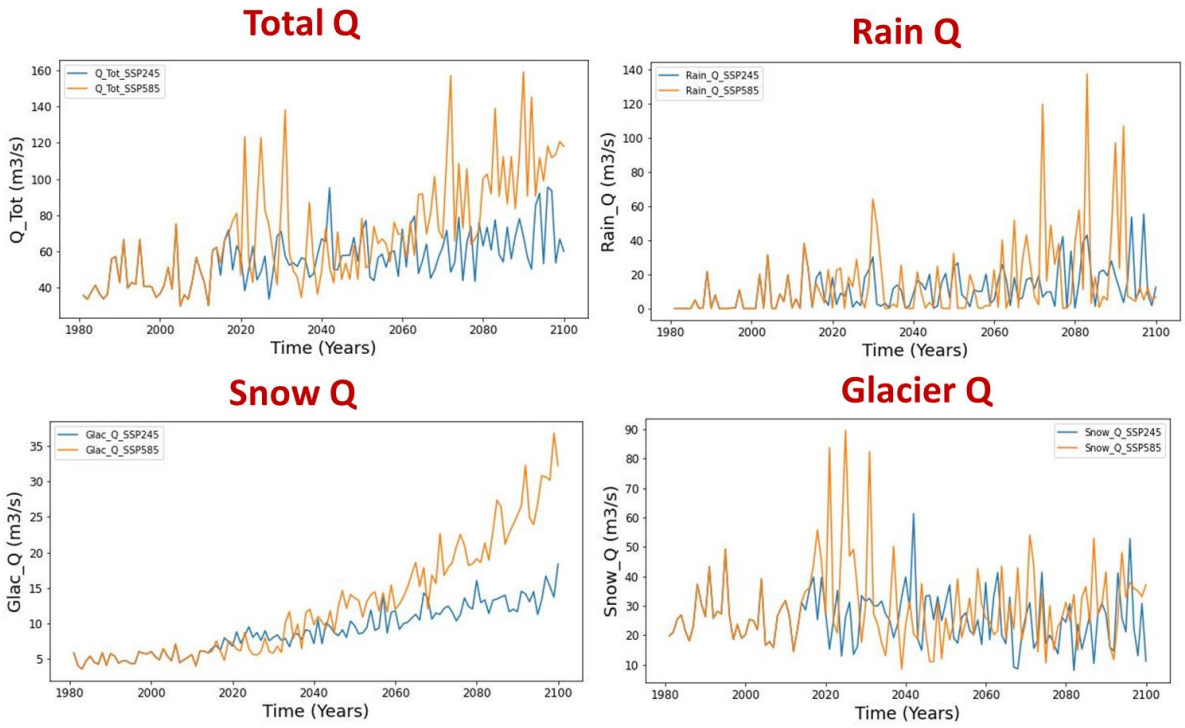

Figure 24: Shows the annual average trends and changes in different runoff components are the Sangla gauge under different CMIP6 scenarios: SSP245 and SSP585.

The Table 8 presents a comparative assessment of different runoff components—Glacial Melt (Glac Q), Snowmelt (Snow Q), Rainfall (Rain Q), and Baseflow (Base Q)—across three time periods: Historical (1981-2014), Near Future Time (NFT, 2021-2050), and Far Future Time (FFT, 2061-2090). It examines the percentage changes in these components between the historical period and the near and far future under two climate scenarios: SSP245 (moderate emissions) and SSP585 (high emissions). The analysis helps reveal how each component of runoff is expected to evolve with climate change and the differing impacts of mitigation efforts.

Under SSP245, glacial melt (Glac Q) is projected to increase by 29.02% in NFT and 51.13% in FFT compared to historical values. This indicates that even under moderate warming, glaciers will contribute significantly more to runoff due to accelerated melting. Snowmelt (Snow Q), on the other hand, shows a decreasing trend, with a reduction of 14.75% in NFT and 44.45% in FFT, suggesting a substantial loss of snow cover over time as temperatures rise (Table 8). Rainfall-derived runoff (Rain Q) is expected to increase by 32.93% in NFT and 84.45% in FFT, indicating more precipitation in the form of rain rather than snow, which is consistent with warming trends. Baseflow (Base Q), representing groundwater contributions, is projected to rise by 28.70% in NFT and 53.16% in FFT, showing that warmer temperatures and increased rainfall will enhance groundwater recharge, though it may also point to changes in permafrost or snowpack dynamics affecting baseflow. Overall, SSP245 reflects a significant shift from snow-driven to rain-driven runoff, with glacial and rainfall contributions increasing over time while snowmelt declines.

Table 8: Shows a comparative assessment of different runoff components—Glacial Melt (Glac Q), Snowmelt (Snow Q), Rainfall (Rain Q), and Baseflow (Base Q)—across three time periods: Historical (1981-2014), Near Future Time (NFT, 2021-2050), and Far Future Time (FFT, 2061-2090).

Stations	Components	Historical, 1981-2014	NFT, 2021-2050	FFT, 2061-2090	% Change (Hist v NFT)	% Change (Hist v FFT)
SSP245	**Glac Q**	11.68	15.07	19.38	29.02	51.13
	Snow Q	58.12	49.55	36.10	-14.75	-44.45
	Rain Q	13.00	17.28	27.59	32.93	84.45
	Base Q	13.08	16.83	22.02	28.70	53.16
SSP585	**Glac Q**	11.68	14.16	20.84	21.25	64.68
	Snow Q	58.12	49.95	31.27	-14.06	-53.77
	Rain Q	13.00	19.83	31.58	52.54	93.73
	Base Q	13.08	16.05	23.91	22.75	67.45

Under the SSP585 scenario, the trends are more pronounced, especially in the far future, reflecting the impact of higher emissions and more severe warming. Glacial melt (Glac Q) increases by 21.25% in NFT and a dramatic 64.68% in FFT, showing that under high emissions, glacier contributions to runoff will be significantly larger, but at the cost of long-term glacier depletion. Snowmelt (Snow Q) sees a 14.06% decrease in NFT and a substantial 53.77% decrease in FFT, indicating that snow-dependent basins will face severe reductions in snow cover, affecting water availability. Rainfall runoff (Rain Q) rises sharply, with a 52.54% increase in NFT and 93.73% in FFT, showing a greater shift towards rainfall-driven runoff, especially in FFT. Baseflow (Base Q) shows an increase of 22.75% in NFT and 67.45% in FFT, indicating greater groundwater contributions due to increased precipitation and potential permafrost thaw under SSP585 (Table 8).

In both scenarios, the increase in glacial melt and rainfall runoff comes at the cost of a substantial reduction in snowmelt, with SSP585 showing more drastic changes. The sharp increases in rainfall-driven runoff and baseflow under SSP585 highlight the greater intensity of hydrological shifts under higher emissions. These changes have critical implications for water resources, as regions dependent on snowmelt may face reduced water availability during summer months, while increased rainfall could lead to more frequent flooding. The data underscores the urgency of climate mitigation, as higher emissions under SSP585 result in far more severe hydrological impacts compared to SSP245, where changes, though significant, are less extreme.

CHAPTER 6

CONCLUSIONS

In the present study, snow/glacier melt contribution and its variation over the years with changes in snow and glaciers in upper Himalayan basin has been analysed. Snow cover area was simulated using the SPHY model and it was found in good agreement with the area obtained using MODIS data. The glacier maps of 2000, 2011 and 2018 have been used to compute the runoff contribution due to glacier melt, snow melt and rain. The runoff from glacier melt found to be 18,15,12%, from snow melt runoff 58,61,64% corresponding to glacier maps of 2000, 2011 and 2018 while rainfall runoff 24% for all the years. Thus, total contribution from snow and glacier melt runoff at the outlet comes out to be 76%. The analysis was also carried out for each month and it was found that there is an increase in total runoff during pre-monsoon and post monsoon months. As per the overall comparative assessment between two time series durations, total runoff has been slightly increased across the basin.

On the basis of analysis of total 17 watersheds (i.e. dominated with snow and glaciers), out of 30 watersheds created on tributaries at the d/s of snow and glacier cover area, it was found that due to glacier recession in the glacier dominated watersheds, glacier melt runoff is reducing. It was found that the watersheds at the lower altitude are reducing glacier cover and thereby runoff have also decreased. In upper part of the basin, the glaciers in the watersheds located on the Northern side are reducing more as compared to the watersheds located on southern side. Therefore, the runoff from watersheds located on Northern side are reducing while it is increasing from the watersheds of the Southern side. Average contribution from these 17 watersheds, glacier melt runoff has decreased 14% and 44%, snow melt increased 24 and 42% and rainfall runoff 31 and 40% for the year 20011 to 2018 with respect to the year 2003. The contribution from rainfall runoff have increased over the years indicating change in precipitation from snow to rain while runoff from snowmelt has increased due to more melting.

As per SPHY, corresponding to glacier map of the year 2000, the glacier ice volume has been computed around 13.41 km^3, while for the glacier map of 2018, it has been reduced around 10.99 km^3.

As per the climate change-based assessment, the comparative assessment of snow cover and runoff components under historical, SSP245, and SSP585 scenarios reveals significant changes driven by climate change. The historical period (1951-2014) shows relatively stable snow cover and runoff patterns, with snowmelt being the dominant source of water. However, projections under SSP245 and SSP585 indicate profound shifts in these dynamics. Under SSP245, moderate emissions lead to a gradual decline in snow cover and snowmelt runoff, with increases in rainfall and glacial melt contributing more significantly to total runoff. Snowmelt decreases by 14.75% and 44.45% in the near and far future, respectively, while glacial melt and rainfall increase substantially. The scenario reflects a slow but steady transition from snow-driven to rain and glacier-driven runoff, particularly after 2050. In contrast, SSP585, with higher emissions, shows much more drastic changes. Snow cover and snowmelt decline sharply, with a 53.77% reduction in snowmelt runoff by 2090. Rainfall and glacial melt increase significantly, especially after mid-century, resulting in more extreme total runoff fluctuations. These trends highlight the amplified hydrological impacts under higher emissions, with intensified rainfall events and accelerated glacier retreat driving future water availability. Overall, the data emphasize the urgent need for climate mitigation to prevent severe reductions in snow cover and to manage the increasing variability in water resources.

Acknowledgement

We thank to National Institute of Hydrology Roorkee for providing all the facilities and data to conduct this study. We also thank you SPHY model developer team Netherlands, USGS NASA team USA and CWC India for providing the software and datasets for the completion of this research work.

REFERENCES

- Abbaspour, K.C., Rouholahnejad, E., Vaghefi, S.R.I.N.I.V.A.S.A.N.B., Srinivasan, R., Yang, H. and Kløve, B., 2015. A continental-scale hydrology and water quality model for Europe: Calibration and uncertainty of a high-resolution large-scale SWAT model. J. Hydrol., 524, pp.733-752.
- Armstrong, R., Alford D., and Racoviteanu, A., (2009): Glaciers as indicators of climate change – the special case of the high elevation glaciers of the Nepal Himalaya. Sustainable mountain development In: International Centre for Integrated Mountain Development (ed.) Water Storage: A Strategy for Climate Change Adaptation in the Himalayas, Winter No. 56. Kathmandu: ICIMOD, 14–16.
- Arnold, J.G., Moriasi, D.N., Gassman, P.W., Abbaspour, K.C., White, M.J., Srinivasan, R., Santhi, C., Harmel, R.D., Van Griensven, A., Van Liew, M.W. and Kannan, N., 2012. SWAT: Model use, calibration, and validation. Transactions of the ASABE, 55(4), pp.1491-1508.
- Barcaza, G., Nussbaumer, S.U., Tapia, G., Valdés, J., García, J.L., Videla, Y., Albornoz, A. and Arias, V., 2017. Glacier inventory and recent glacier variations in the Andes of Chile, South America. Annals of Glaciology, 58(75pt2), pp.166-180.
- Bhambri, R. and T. Bolch., (2009): Glacier mapping: a review with special reference to the Indian Himalayas. Progress in Physical Geography, 33(5), 672–704.
- Bhambri, R., T. Bolch, R.K. Chaujar, S.C. Kulshreshtha., (2011): Glacier changes in the Garhwal Himalaya, India, from 1968 to 2006 based on remote sensing, Journal of Glaciology, 203(57), 543-556.
- Bhutiyani, M.R., V.S. Kale and N.J. Pawar, (2007): Long-term trends in maximum, minimum and mean annual air temperatures across the North-western Himalaya during the twentieth century. Climatic Change, 85(1–2), 159–177.

- Bhutiyani, M.R., V.S. Kale and N.J. Pawar, (2009): Climate change and the precipitation variations in the north-western Himalaya: 1866–2006. International Journal of Climatology, 30(4), 535–548.
- Bishop, M.P. and J.F. Shroder., Jr., (eds): (2004): Geographic Information Science and Mountain Geomorphology. Springer-Praxis, Chichester.
- Bishop, M.P., J.F. Shroder, Jr. B. L. Hickman., and L. Copland, (1998): Scale dependent analysis of satellite imagery for characterization of glacier surfaces in the Karakoram Himalaya. Geomorphology 21, 217–232.
- Bliss, A., Hock, R. and Radić, V., 2014. Global response of glacier runoff to twenty-first century climate change. Journal of Geophysical Research: Earth Surface, 119(4), pp.717-730.
- Bogorodskiy, V.V., V.C. Bentley, and P.E. Gudmandsen, (1985): Radio glaciology, Reidel, Dordrecht, Holland, Reidel Publ. Company.
- Bolch T. and U. Kamp, (2006): Glacier mapping in high mountains using DEMs, Landsat and ASTER data. In Kaufmann, V. And W. Sulzer, (eds): Proceedings of the 8th International Symposium on High Mountain Remote Sensing Cartography. Graz, Karl Franzens University, 13–24. (Grazer Schriften der Geographie und Raumforschung 41.)
- Bolch T., T. Yao, S. Kang, M.F. Buchroithner., D. Scherer, F. Maussion, E. Huintjes and C. Schneider., (2010): A glacier inventory for the western Nyainqentanglha Range and the Nam Co Basin, Tibet, and glacier changes 1976-2009, The Cryosphere, 4, 419–433, doi: 10.5194/tc-4-419-2010.
- Bolch, T., B. Menounos, R. Wheate., (2010): Landsat-based inventory of glaciers in western Canada, 1985–2005, Remote Sensing of Environment 114 (2010), 127–137.

- Bolch, T., Kulkarni, A., Kääb, A., Huggel, C., Paul, F., Cogley, J.G., Frey, H., Kargel, J.S., Fujita, K., Scheel, M. and Bajracharya, S., 2012. The state and fate of Himalayan glaciers. Science, 336(6079), pp.310-314.
- Bolch, T., M. Buchroithner, T. Pieczonka and A. Kunert., (2008): Planimetric and volumetric glacier changes in the Khumbu Himal, Nepal, since 1962 using Corona, Landsat TM and ASTER data. Journal of Glaciology, 54(187), 592–600.
- Bolch, T., M.F Buchroithner, A. Kunert and U. Kamp, (2007): Automated delineation of debris-covered glaciers based on ASTER data. In Gomarasca, M.A., ed. GeoInformation in Europe. Proceedings of the 27th EARSeL Symposium, 4–6 June 2007, Bolzano, Italy. Rotterdam, Millpress, 403–410.
- Burger, F., Brock, B. and Montecinos, A., 2018. Seasonal and elevational contrasts in temperature trends in Central Chile between 1979 and 2015. Global and planetary change, 162, pp.136-147.
- Bush, A.B.G., (2000): A positive feedback mechanism for Himalayan glaciations. Quaternary International, 65(6), 3–13.
- Byers, E., Gidden, M. and Maussion, F., 2017. Working with big, multi-dimensional geoscientific datasets in Python: a tutorial introduction to xarray.
- Cannon, A.J., Sobie, S.R. and Murdock, T.Q., 2015. Bias correction of GCM precipitation by quantile mapping: how well do methods preserve changes in quantiles and extremes? Journal of Climate, 28(17), pp.6938-6959.
- Chaohai, L. and Sharma, C.K., (1988): Report on first expedition to glaciers in the Pumqu (Arun) and Poiqu (Bhote-Sun Kosi) river basins, Xizang (Tibet), China. Science Press, Beijing, p. 192.
- Chaujar, R.K., (2009): Climate change and its impact on the Himalayan glaciers – a case study on the Chorabari glacier, Garhwal Himalaya, India. Current Science, 96(5), 703–707.

- Clarke, G.K., Jarosch, A.H., Anslow, F.S., Radić, V. and Menounos, B., 2015. Projected deglaciation of western Canada in the twenty-first century. Nature Geoscience, 8(5), pp.372-377.
- Colbeck, S.C., (1988): Snowmelt increase through albedo reduction, Proc. of Workshop on Snow Hydrology, held at Manali from Nov. 23-26 pp. VI-12.
- de Boer, F., 2016. HiHydroSoil: A high resolution soil map of hydraulic properties. Wageningen, the Netherlands, 20.
- Demuth, M.N., Wilson, P. and Haggarty, D., 2014. Glaciers of the Ragged Range, Nahanni National Park Reserve, Northwest Territories, Canada. In Global land ice measurements from space (pp. 375-383). Springer, Berlin, Heidelberg.
- Dimri, A.P., Kumar, D., Choudhary, A. and Maharana, P., 2018. Future changes over the Himalayas: mean temperature. Global and planetary change, 162, pp.235-251.
- Dyhrenfurth, G.O., (1955): TO THE THIRD POLE. Dyhrenfurth, London, 1st edition Chipped DJ Fine.
- Dyurgerov, M.B., Meier, M.F., (1997): Mass balance of mountain and sub polar glaciers: a new global assessment for 1961–1990. Arctic and Alpine Research 29 (4), 379–391.
- Engelhardt, M., Ramanathan, A.L., Eidhammer, T., Kumar, P., Landgren, O., Mandal, A. and Rasmussen, R.O.Y., 2017. Modelling 60 years of glacier mass balance and runoff for Chhota Shigri Glacier, Western Himalaya, Northern India. J. Glaciol., 63(240), pp.618-628.
- Falaschi, D., Bravo, C., Masiokas, M., Villalba, R. and Rivera, A., 2013. First glacier inventory and recent changes in glacier area in the Monte San Lorenzo Region (47 S), Southern Patagonian Andes, South America. Arctic, Antarctic, and Alpine Research, 45(1), pp.19-28.

- Farinotti, D., Longuevergne, L., Moholdt, G., Duethmann, D., Mölg, T., Bolch, T., Vorogushyn, S. and Güntner, A., 2015. Substantial glacier mass loss in the Tien Shan over the past 50 years. Nature Geoscience, 8(9), pp.716-722.
- Flint, R. F., (1964): Glacial and Quaternary Geology, John Wiley, pp. 63–85.
- Geological Survey of India, 1907. Preliminary survey of certain glaciers in North-West Himalaya. Records of the Geological Survey of India, 35: 123-126.
- Gupta, V., Jain, M.K., Singh, P.K. and Singh, V., 2019. An assessment of global satellite-based precipitation datasets in capturing precipitation extremes: A comparison with observed precipitation dataset in India. International Journal of Climatology. https://doi.org/10.1002/joc.6419.
- Haeberli, W. and Beniston, M., (1998): Climate change and its impacts on glaciers and permafrost in the Alps. Ambio, 27 (4), 258–265.
- Haeberli, W., Hoelzle, M., Suter, S. (eds.) (1998): Historical evolution and operational aspects of worldwide glacier monitoring. Into the second century of worldwide glacier monitoring: Prospects and Strategies. Studies and Reports in Hydrology. UNESCO, Paris: p.35–51.
- Hall, D. K. and G. A. Riggs. 2016. *MODIS/Terra Snow Cover 8-Day L3 Global 500m SIN Grid, Version 6*. [Indicate subset used]. Boulder, Colorado USA. NASA National Snow and Ice Data Center Distributed Active Archive Center. https://doi.org/10.5067/MODIS/MOD10A2.006. [Date Accessed]
- Hall, D.K., G.A. Riggs and V.V. Salomonson., (1995): Development of methods for mapping global snow covers using Moderate Resolution Imaging Spectroradiometer (MODIS) data. Remote Sensing of Environment, **54**(2), 127–140.
- Huss, M. and Hock, R., 2018. Global-scale hydrological response to future glacier mass loss. Nature Climate Change, 8(2), pp.135-140.

- Immerzeel, W.W. and Bierkens, M.F.P., 2012. Asia's water balance. Nature Geoscience, 5(12), p.841-842.
- Immerzeel, W.W., Droogers, P., De Jong, S.M. and Bierkens, M.F.P., 2009. Large-scale monitoring of snow cover and runoff simulation in Himalayan river basins using remote sensing. Remote sensing of Environment, 113(1), pp.40-49.
- Immerzeel, W.W., Kraaijenbrink, P.D.A., Shea, J.M., Shrestha, A.B., Pellicciotti, F., Bierkens, M.F.P. and De Jong, S.M., 2014. High-resolution monitoring of Himalayan glacier dynamics using unmanned aerial vehicles. Remote Sensing of Environment, 150, pp.93-103.
- Immerzeel, W.W., L.P.H. van Beeke and M.F.P. Bierkens., (2010). Climate change will affect the Asian water towers. Science, 328(5984), 1382–1385.
- Immerzeel, W.W., Van Beek, L.P. and Bierkens, M.F., 2010. Climate change will affect the Asian water towers. Science, 328(5984), pp.1382-1385.
- Jain, S.K., Tyagi, J. and Singh, V., 2010. Simulation of runoff and sediment yield for a Himalayan watershed using SWAT model. Journal of Water Resource and Protection, 2(3), 267-281.
- Ka¨a¨b, A., (2002): Monitoring high-mountain terrain deformation from repeated air- and spaceborne optical data: examples using digital aerial imagery and ASTER data. *ISPRS* Journal of Photogrammetry and Remote Sensing, **57**(1–2), 39–52.
- Kadota, T., Seko, K., Aoki, T., Iwata, S. & Yamaguchi, S., (2000): Shrinkage of Khumbu Glacier, east Nepal from 1978 to 1995, IAHS Publication 264, 235–243.
- Kargel, J.S., Abrams, M.J., Bishop, M.P., (2005): Multispectral imaging contributions to global land ice measurements from space. Remote Sensing of Environment, 99, 187–219.
- Kollmeyer, R.C., (1980): West Greenland outlet glaciers: an inventory of the major iceberg producers. Cold Regions Science and Technology, 1, 175–181.

- Kotlyakov, V.M., Serebrjanny, L.R., and Solomina, O.N., (1991): Climate change and glacier fluctuations during the last 1,000 years in the southern mountains of the USSR. Mountain Research and Development, 11, 1–12.
- Kozhikkodan Veettil, B. and de Souza, S.F., 2017. Study of 40-year glacier retreat in the northern region of the Cordillera Vilcanota, Peru, using satellite images: preliminary results. Remote Sensing Letters, 8(1), pp.78-85.
- Kraaijenbrink, P.D.A., Bierkens, M.F.P., Lutz, A.F. and Immerzeel, W.W., 2017. Impact of a global temperature rise of 1.5 degrees Celsius on Asia's glaciers. Nature, 549(7671), pp.257-260.
- Kulkarni A.V. and S. Alex, (2003): Estimation of Recent Glacial Variations in Baspa Basin Using Remote Sensing Technique. Journal of the Indian Society of Remote Sensing, 31(2), 81-90.
- Kulkarni, A.V. and Bahuguna, I.M., (2002): Glacial retreat in the Baspa basin, Himalayas, monitored with satellite stereo data. Journal of Glaciology, 48, 171–172.
- Kulkarni, A.V. and Buch, A.M., (1991): Glacier Atlas of Indian Himalaya, Scientific Note: SAC/RSA/RSAG-MWRD/SN/05/91, Space Applications Centre, Ahmedabad.
- Kulkarni, A.V. and Karyakarte, Y., 2014. Observed changes in Himalayan glaciers. Current Science, pp.237-244.
- Kulkarni, A.V., 2012. Monitoring Himalayan cryosphere using remote sensing techniques. Journal of the Indian Institute of Science, 90(4), pp.457-469.
- Kulkarni, A.V., B.P. Rathore, S. Mahajan and P. Mathur., (2005): Alarming retreat of Parbati glacier, Beas basin, Himachal Pradesh. Current Science, 88(11), 1844–1850.
- Kulkarni, A.V., Bahuguna, I.M., Rathore, B.P., Singh, S.K., Randhawa, S.S., Sood, R.K. and Dhar, S., 2007. Glacial retreat in Himalaya using Indian remote sensing satellite data. Current science, pp.69-74.

- Kulkarni, A.V., Bhauguna I.M., Rathore B.P., Singh S.K., Randhawa S.S., Sood R.K., (2007): Glacial retreat in Himalaya using Indian remote sensing satellite data. Current Science, 92(1), 69–74.
- Kumar, A., Tiwari, S.K., Verma, A. and Gupta, A.K., 2018. Tracing isotopic signatures (δD and δ18O) in precipitation and glacier melt over Chorabari Glacier–Hydroclimatic inferences for the Upper Ganga Basin (UGB), Garhwal Himalaya. J. Hydrol.: Regional Studies, 15, pp.68-89.
- Li, Z., Sun, W. and Zeng, Q., (1998): Measurements of glacier variation in the Tibetan Plateau using Landsat data. Remote Sensing of Environment, 63, 258–64.
- Lutz, A.F., Immerzeel, W.W., Shrestha, A.B. and Bierkens, M.F.P., 2014. Consistent increase in High Asia's runoff due to increasing glacier melt and precipitation. Nature Climate Change, 4(7), pp.587-592.
- Maisch, M., (2000): The long-term signal of climate change in the Swiss Alps: glacier retreat since the end of the Little Ice Age and future ice decay scenarios. Geogr. Fı´s. Din. Quat., 23(2), 139–151.
- Malmros, J.K., Mernild, S.H., Wilson, R., Yde, J.C. and Fensholt, R., 2016. Glacier area changes in the central Chilean and Argentinean Andes 1955–2013/14. J. Glaciol., 62(232), pp.391-401.
- Mayewski, P.A. and P.A. Jeschke., (1979): Himalayan and trans-Himalayan glacier fluctuations since A.D. 1812. Arctic and Alpine Research, 11(3), 267–287.
- Mehta M., D.P. Dobhal, Bisht M.P.S., (2011): Change in Tipra glacier in the Gharwal Himalay India, between 1962 and 2008. Progress in Physical Geography, 35(6) 721-738.
- Meier, M.F. and Wahr, J.M., (2002): Sea level is rising: Do we know why? Proceedings of the National Academy of Science 99 (10), 6524–6526.

- Mir, R.A., Jain, S.K., Jain, S.K., Thayyen, R.J. and Saraf, A.K., 2017. Assessment of recent glacier changes and its controlling factors from 1976 to 2011 in Baspa basin, western Himalaya. Arctic, antarctic, and alpine research, 49(4), pp.621-647.
- Mool, P.K., Wangda, D., Bajracharya, S.R., Joshi, S.P., Kujzang, K., and Gurung, D.R. (2001): Inventory of Glaciers, Glacial Lakes and Glacial Lake Outburst Flood Monitoring and Early Warning System in the Hindu Kush-Himalayan Region, Bhutan 227. ICIMOD in cooperation with UNEP/ RRC-AP, ISBN 92 9115 3451, Published by ICIMOD, Kathmandu, Nepal.
- Muller, F., (1980): Glaciers and their fluctuations, Nature and Resources, 16(2): 5-11.
- Muller, F., Caflisch, T and Muller,G., (1977): Instructions for compilation and assemblage of data for a World Glacier Inventory, Dept. of Geography, Swiss Federal Institute of Technology, Zurich.
- Nainwal, H.C., K.S. Sajwan, I.M. Bahuguna and A.V. Kulkarni., (2008): Monitoring of recession of the glaciers using satellite data: a case study from Saraswati (Alaknanda) Basin, Garhwal Himalaya. In Proceedings of National Seminar on Glacial Geomorphology and Palaeoglaciation in Himalaya, 13–14 March 2008.
- Nakawo, M., Fujita, K., Ageta, U., (1997): Basic studies for assessing the impacts of the global warming on the Himalayan cryosphere. Bulletin of Glacier Research, 15, 53–58.
- Narod B.B. and Clarke G.K.C., (1994): Miniature high-power impulse transmitter for radio-echo sounding. Journal of Glaciology, 40(134). 190-194.
- Oerlemans, J., (1994): Quantifying global warming from the retreat of glaciers. Science, 264, 243-245.
- Ouma O. Y., Tateishi R., (2005): Optical satellite-sensor based monitoring of glacial coverage fluctuations on Mount Kenya, 1987-2000, International Journal of Environmental Studies, 62, 663-673.

- Pan B., Zhang G., Wang J., Cao B., Wang J., Zhang C., Geng H., and Ji Y., (2011): Glacier changes from 1966–2009 in the Gongga Mountains, on the south-eastern margin of the Qinghai-Tibetan Plateau and their climatic forcing, The Cryosphere Discuss, 5, 3479–3516.
- Paul F., (2002): Changes in glacier area in Tyrol, Austria, between 1969 and 1992 derived from Landsat 5 thematic Mapper and Austrian Glacier Inventory data, International Journal of Remote Sensing, 23(4), 787-799.
- Paul, F.R., Barry, R.G., Cogley, J.G., Frey, H., Haeberli, W., Ohmura, A., Ommanney, C. S. L., Raup, B., Rivera, A., and Zemp, M., (2009): Recommendations for the compilation of glacier inventory data from digital sources, Ann. Glaciol., 50(53), 119–126,
- Prakash, S., 2019. Performance assessment of CHIRPS, MSWEP, SM2RAIN-CCI, and TMPA precipitation products across India. J. Hydrol., 571, pp.50-59.
- Prasad, V., Kulkarni, A.V., Pradeep, S., Pratibha, S., Tawde, S.A., Shirsat, T., Arya, A.R., Orr, A. and Bannister, D., 2019. Large losses in glacier area and water availability by the end of twenty-first century under high emission scenario, Satluj basin, Himalaya. Current Science, 116(10), 1721-1730.
- Price, R. J., (1973): Glacial and Fluvioglacial Landforms (ed. Clayton, K. M.), Oliver and Boyd, pp. 20–41.
- Rabatel, A., Sanchez, O., Vincent, C. and Six, D., 2018. Estimation of glacier thickness from surface mass balance and ice flow velocities: a case study on Argentière Glacier, France. Frontiers in Earth Science, 6, p.112.
- Racoviteanu, A., F. Paul, B. Raup, S.J.S. Khalsa and R. Armstrong (2009): "Challenges and recommendations in mapping of glacier prameters from space: results of the 2008 Global Land Ice Measurements frpom Space (GLIMS) workshop, Boulder, Colorado, USA." Annals of Glaciology 50(53).

- Racoviteanu, A.E., Y. Arnaud, M.W. Williams and J. Ordon˜ ez., (2008): Decadal changes in glacier parameters in the Cordillera Blanca, Peru, derived from remote sensing. Journal of Glaciology, 54(186), 499–510.
- Raina, V.K. and D. Srivastava., (2008): Glacier atlas of India. Bangalore, Geological Society of India.
- Rao, M.P., Cook, E.R., Cook, B.I., Palmer, J.G., Uriarte, M., Devineni, N., Lall, U., D'Arrigo, R.D., Woodhouse, C.A., Ahmed, M. and Zafar, M.U., 2018. Six centuries of Upper Indus Basin streamflow variability and its climatic drivers. Water Resour. Res., 54(8), pp.5687-5701.
- Raup, B., A. Racoviteanu, S.J.S. Khalsa, C. Helm, R. Armstrong and Y. Arnaud., (2007): The GLIMS geospatial glacier database: a new tool for studying glacier change. Global and Planetary Change, 56(1–2), 101–110.
- Ren, J., Jing, Z., Pu, J. & X. Qin., (2006): Glacier variations and climate change in the central Himalaya over the past few decades. Annals of Glaciology, 43, 218-222.
- Ren, Y.Y., Ren, G.Y., Sun, X.B., Shrestha, A.B., You, Q.L., Zhan, Y.J., Rajbhandari, R., Zhang, P.F. and Wen, K.M., 2017. Observed changes in surface air temperature and precipitation in the Hindu Kush Himalayan region over the last 100-plus years. Advances in Climate Change Research, 8(3), pp.148-156.
- Romshoo, S.A., Dar, R.A., Rashid, I., Marazi, A., Ali, N. and Zaz, S.N., 2015. Implications of shrinking cryosphere under changing climate on the streamflows in the Lidder catchment in the Upper Indus Basin, India. Arctic, antarctic, and alpine research, 47(4), pp.627-644.
- Rott, H., (1994): Thematic studies in alpine areas by means of polarimetric SAR and optical imagery. Advances in Space Research, **14**(3), 217–226.

- Sanjay, J., Krishnan, R., Shrestha, A.B., Rajbhandari, R. and Ren, G.Y., 2017. Downscaled climate change projections for the Hindu Kush Himalayan region using CORDEX South Asia regional climate models. Advances in Climate Change Research, 8(3), pp.185-198.
- Schaner, N., Voisin, N., Nijssen, B. and Lettenmaier, D.P., 2012. The contribution of glacier melt to streamflow. Environmental Research Letters, 7(3), p.034029. https://iopscience.iop.org/article/10.1088/1748-9326/7/3/034029
- Schneider, C., M. Schnirch, C. Acun˜ a, G. Casassa and R. Kilian., (2007): Glacier inventory of the Gran Campo Nevado Ice Cap in the Southern Andes and glacier changes observed during recent decades. Global and Planetary Change, 59(1–4), 87–100.
- Seltzer, G.O., (1993): Late-quaternary glaciations as a proxy for climate change in the central Andes. Mountain Research and Development, 13, 129–138.
- Shafiq, M.U., Bhat, M.S., Rasool, R., Ahmed, P., Singh, H. and Hassan, H., 2016. Variability of Precipitation regime in Ladakh region of India from 1901-2000. J Climatol Weather Forecasting, 4(165), p.2.
- Sharma, A. and Goyal, M.K., 2020. Assessment of the changes in precipitation and temperature in Teesta River basin in Indian Himalayan Region under climate change. Atmospheric Research, p.104670. https://doi.org/10.1016/j.atmosres.2019.104670.
- Shroder, J.F. Jr. and Bishop, M.P., (2000): Unroofing of the Nanga Parbat Himalaya. In: Khan, M.A., Treloar, P.J., Searle, M.P., and Jan, M.Q. (Eds), Tectonics of the Nanga Parbat Syntaxis and the Western Himalaya. Geological Society, London, 170, 163–179.
- Shukla, A., Arora, M.K. and Gupta, R.P., 2010. Synergistic approach for mapping debris-covered glaciers using optical–thermal remote sensing data with inputs from geomorphometric parameters. Remote Sensing of Environment, 114(7), pp.1378-1387.

- Shukla, S., Kansal, M.L. and Jain, S.K., 2017. Snow cover area variability assessment in the upper part of the Satluj river basin in India. Geocarto International, 32(11), pp.1285-1306.
- Sidjak, R.W. and R.D. Wheate., (1999): Glacier mapping of the Illecillewaet ice field, British Columbia, Canada, using Landsat TM and digital elevation data. International Journal of Remote Sensing, 20(2), 273–284.
- Silverio, W. and J.M. Jaquet., (2005): Glacial cover mapping (1987– 1996) of the Cordillera Blanca (Peru) using satellite imagery. Remote Sensing of Environment, 95(3), 342–350.
- Singh, P. and Jain, S.K., 2002. Snow and glacier melt in the Satluj River at Bhakra Dam in the western Himalayan region. Hydrological Sciences Journal, 47(1), pp.93-106.
- Singh, P., Arora, M. and Goel, N.K., 2006. Effect of climate change on runoff of a glacierized Himalayan basin. Hydrological Processes: An International Journal, 20(9), pp.1979-1992.
- Singh, P., L. Polglase and D.Wilson., (2009): Role of snow and glacier melt runoff modeling in hydropower projects in the Himalayan region. In Jain, S.K., V.P. Singh, V. Kumar, R. Kumar, R.D. Singh and K.D. Sharma, eds. Proceedings of the International Conference on Water, Environment, Energy and Society (WEES–2009), 12–16 January 2009, New Delhi, India. Vol. 1. Roorkee, National Institute of Hydrology, 366–371.
- Singh, V. and Goyal, M.K., 2016. Analysis and trends of precipitation lapse rate and extreme indices over north Sikkim eastern Himalayas under CMIP5ESM-2M RCPs experiments. Atmospheric Research, 167, pp.34-60.
- Singh, V. and Goyal, M.K., 2017. Curve number modifications and parameterization sensitivity analysis for reducing model uncertainty in simulated and projected streamflows

in a Himalayan catchment. Ecological Engineering, 108, pp.17-29. https://doi.org/10.1016/j.ecoleng.2017.08.002

- Singh, V. and Goyal, M.K., 2018. An improved coupled framework for Glacier classification: an integration of optical and thermal infrared remote-sensing bands. International journal of remote sensing, 39(20), pp.6864-6892.
- Singh, V. and Xiaosheng, Q., 2019. Data assimilation for constructing long-term gridded daily rainfall time series over Southeast Asia. Climate Dynamics, 53(5-6), pp.3289-3313.
- Solomon, S. Qin, M. Manning, Z. Chen, M. Marquis, K.B. Averyt, M. Tignor and H.L. Miller (eds.) (2007): Climate change 2007: the physical science basis. Contribution of Working Group I to the Fourth Assessment Report of the Intergovernmental Panel on Climate Change. Cambridge, etc., Cambridge University Press. Cambridge, United Kingdom and New York, NY, USA, 996 pp.
- Strozzi, T., Wegmüller, U., Perruchoud, E., Delaloye, R., Kääb, A., Ambrosi, C., (2008): Evolution of a deep-seated rock mass movement observed with satellite SAR interferometry. Proceedings of the FRINGE 2007 Workshop, Frascati, Italy, 26-30 November 2007, (ESA SP-649).
- Terink, W., Lutz, A.F., Immerzeel, W., Nepal, S., Khanal, S. and Shrestha, A.B., 2016, December. Improvement of the SPHY Model Glacier Module and its Application in the Tamakoshi River Basin, Nepal. In AGU Fall Meeting Abstracts.
- Terink, W., Lutz, A.F., Simons, G.W.H., Immerzeel, W.W. and Droogers, P., 2015. SPHY v2. 0: Spatial processes in Hydrology. Geoscientific Model Development, 8(7), pp.2009-2034.
- Thayyen, R.J. and Gergan, J.T., 2010. Role of glaciers in watershed hydrology: a preliminary study of a" Himalayan catchment". The Cryosphere, 4(1), p.115-128.

- Tucker C.J., Grant D.M., Dykstra J.D., (2004): NASA's Global Orthorectified Landsat Data Set. Photogrammetric Engineering & Remote Sensing, 70, 313-322.
- Weidinger, J., Gerlitz, L., Bechtel, B. and Böhner, J., 2018. Statistical modelling of snow cover dynamics in the Central Himalaya Region, Nepal.
- WWF, (2005): An Overview of Glaciers, Glacier Retreat, and Subsequent Impacts in Nepal, India and China. WWF Nepal Program: pp. 79.
- Xu, J., Grumbine, R.E., Shrestha, A., Eriksson, M., Yang, X., Wang, Y.U.N. and Wilkes, A., 2009. The melting Himalayas: cascading effects of climate change on water, biodiversity, and livelihoods. Conservation Biology, 23(3), pp.520-530.
- Zemp, M., Huss, M., Thibert, E., Eckert, N., McNabb, R., Huber, J., Barandun, M., Machguth, H., Nussbaumer, S.U., Gärtner-Roer, I. and Thomson, L., 2019. Global glacier mass changes and their contributions to sea-level rise from 1961 to 2016. Nature, 568(7752), pp.382-386.
- Zhao, W., He, J., Wu, Y., Xiong, D., Wen, F. and Li, A., 2019. An analysis of land surface temperature trends in the Central Himalayan region based on MODIS products. Remote Sensing, 11(8), p.900. https://doi.org/10.3390/rs11080900.